

Ion channel gating in cardiac ryanodine receptors from the arrhythmic RyR2-P2328S mouse

Samantha C. Salvage^{1,2}, Esther M. Gallant³, Nicole A. Beard⁴; Shiraz Ahmad¹, Haseeb Valli¹, James A. Fraser¹; Christopher L.-H Huang^{1,2}; Angela F. Dulhunty³

- ¹. Physiological Laboratory, University of Cambridge, Downing Street, Cambridge, CB2 3EG, UK.
- ². Department of Biochemistry, University of Cambridge, Tennis Court Road, Cambridge, CB2 1QW, UK.
- ³. Eccles Institute of Neuroscience, John Curtin School of Medical Research, 131 Garran Road, The Australian National University, Acton ACT 2601, Australia
- ⁴. Centre for Research in Therapeutic Solutions, Faculty of Science and Technology, University of Canberra, Bruce, ACT 2617, Australia.

Corresponding Author:

angela.dulhunty@anu.edu.au

Key words: RyR2 P2328S ion channels; P2328S-RyR2 mouse; atrial fibrillation; catecholaminergic polymorphic ventricular tachycardia; cytoplasmic Ca²⁺ activation and inactivation; FKBP and phosphorylation.

Summary Statement

The RyR2-P2328S mutation, precipitating potentially fatal arrhythmia in humans, can be attributed to leftward shifts in cytoplasmic Ca²⁺-dependent RyR2 activation and inactivation in the absence of adrenergic stimulation.

Abstract

Mutations in the cardiac ryanodine receptor calcium release channel (RyR2) can cause deadly ventricular arrhythmias and atrial fibrillation (AF). The RyR2-P2328S mutation produces catecholaminergic polymorphic ventricular tachycardia (CPVT) and AF in hearts from RyR2^{P2328S/P2328S} (RyR2^{S/S}) mice. We have now examined P2328S RyR2 channels from RyR2^{S/S} hearts. The activity of wild type (WT) and P2328S RyR2 channels was similar at a cytoplasmic [Ca²⁺] of 1 mM, but P2328S RyR2 was significantly more active than WT at a cytoplasmic [Ca²⁺] of 1 μM. This was associated with a >10-fold shift in the AC₅₀ for Ca²⁺-activation from ~3.5 μM Ca²⁺ in WT RyR2 to ~320 nM in P2328S channels and an unexpected >1000-fold shift in the IC₅₀ for inactivation from ~50 mM in WT channels to ≤7 μM in P2328S channels, into systolic [Ca²⁺] levels. Unexpectedly, the shift in Ca²⁺-activation was not associated with changes in subconductance activity, S2806 or S2814 phosphorylation, or FKBP12 bound to the channels. The changes in channel activity with the P2328S mutation correlate with altered Ca²⁺ homeostasis in myocytes from RyR2^{S/S} mice and the CPVT and AF phenotypes.

List of symbols and abbreviations

AF - atrial fibrillation

AC₅₀ – Ca²⁺ concentration for 50% activation

BP_A - baseline P_o at [Ca²⁺] less than activating levels

BP_I – baseline P_o that [Ca²⁺]-inactivation decayed towards

CLIC-2 – chloride intracellular ion channel type 2

CPVT – catecholaminergic polymorphic ventricular tachycardia

DAD –delayed after-depolarisation

F_o – frequency of open events

H_A - Hill coefficient for Ca²⁺- dependent activation

H_I - Hill coefficient for Ca²⁺- dependent inactivation

IC₅₀ – Ca²⁺ concentration at 50% inhibition

NCX - Sodium calcium exchanger

P_o – probability of the channel being open

RyR2 – cardiac isoform of the ryanodine receptor

T_o – mean channel open time

T_c – mean channel closed time

SR – sarcoplasmic reticulum

VF – ventricular fibrillation

WT – wild type

Introduction

Mammalian heart rhythm depends on the activity of ion channels, ion transporters and Ca²⁺ binding proteins in the surface membrane, cytoplasm and intracellular sarcoplasmic reticulum (SR) Ca²⁺ store of cardiac myocytes. The intracellular Ca²⁺ handling proteins control Ca²⁺ release and contraction during systole, as well as diastolic Ca²⁺ re-uptake and storage in the SR. Mutations or acquired changes in these proteins lead to arrhythmia and heart failure (Bers, 2001). Mutations in the cardiac ryanodine receptor (RyR2), the ligand-gated SR Ca²⁺ release channel, can increase channel open probability during diastole, resulting in excess diastolic SR Ca²⁺ release, and leading to catecholaminergic polymorphic ventricular tachycardia (CPVT) (Laitinen et al., 2001; Lehnart et al., 2004; Priori et al., 2001; Swan et al., 1999), ventricular fibrillation (VF) (Cerrone et al., 2005; Jiang et al., 2007; Paech et al., 2014) or atrial fibrillation (AF) (Pizzale et al., 2008; Sumitomo et al., 2007). CPVT is an inherited channelopathy, characterised by often-fatal ventricular tachycardia exacerbated by physical or emotional adrenergic stress. More than 150 different mutations to date in RyR2 disturb ion channel function and account for 70% - 80% of CPVT cases. The mutations lead to abnormal SR Ca²⁺ handling and subsequent pro-arrhythmic SR Ca²⁺ ‘leak’ (Priori and Chen, 2011; Ronen and Lili, 2016; Sumitomo, 2016). In contrast to the typically monogenic nature of CPVT, VF and AF are multifactorial, but can also involve disrupted Ca²⁺ homeostasis. AF is the most common sustained arrhythmia, resulting in significant clinical morbidity and mortality (Benjamin et al., 1998; Davis et al., 2012; Kourliouros et al., 2009). Abnormally high diastolic cytoplasmic [Ca²⁺]_i trigger the surface membrane sodium calcium exchanger (NCX) to extrude Ca²⁺, generating a delayed after-depolarisation (DAD) as NCX imports three Na⁺ ions for every Ca²⁺ extruded. Triggered, arrhythmogenic action potentials are generated when the DAD reaches action potential threshold.

The molecular properties of RyR2 carrying CPVT and/or AF mutations which lead to diastolic Ca²⁺ leak are frequently studied using RyR2 channels expressed in HEK 293 cells (Jiang et al., 2005; Liu et al., 2013; Meli et al., 2011; Paavola et al., 2007). Mammalian models of RyR2 mutations are particularly useful because the ion channel is subjected to many post-translational modifications that also occur in patients, but only a few have been developed (Cerrone et al., 2005; Goddard et al., 2008; Lehnart et al., 2008; Shan et al., 2010; Shan et al., 2012). An advantage of animal models is that the ion channel properties can be directly correlated with changes in heart function and susceptibility to arrhythmia (Huang, 2017).

The RyR2-P2328S mutation is one of a few CPVT-related mutations that has been reported to also be associated with AF (Glukhov et al., 2015; Goddard et al., 2008; King et al., 2013; Laitinen et al., 2001; Lehnart et al., 2004; Salvage et al., 2015; Xiao et al., 2016; Zhang et al., 2011). We have generated a mouse model of the P2328S mutation; RyR2^{P2328S/P2328S} (RyR2^{S/S}) (Goddard et al., 2008). The mutation lies within an RyR2 mutation ‘hot-spot’; Domain II or the central region, encompassing amino acids 2246-2534 which are conserved across species and isoforms (Yano et al., 2005), is included in the HD1 domain of RyR2 (Dhindwal et al., 2017). The RyR2^{S/S} mouse demonstrates the atrial and ventricular arrhythmic phenotype seen in patients (Goddard et al., 2008; Sabir et al., 2010; Zhang et al., 2011). The arrhythmia is associated with reduced action potential conduction velocity, reduced expression of Nav1.5 and reduced Na⁺ channel function (King et al.,

2013; Ning et al., 2016; Salvage et al., 2015; Zhang et al., 2013). It is also associated with DAD phenomena (King et al., 2013), suggesting that RyR2 may be hyperactive. Indeed increased RyR2 sensitivity to cytosolic Ca^{2+} was indicated in a study of cellular Ca^{2+} handling (Goddard et al., 2008). P2328S RyR2 channels expressed in HEK 293 cells show increased activity at 150 nM cytoplasmic Ca^{2+} , but only after PKA activation led to increased phosphorylation and reduced FKBP binding and (Lehnart et al., 2004). Thus, in addition to its clinical phenotype, the P2328S mutation is of interest because of this reported loss of regulatory 12.6 kDa FK506 binding protein (FKBP 12.6). In this context, the mutation is in the general proximity of a putative, albeit controversial, FKBP12/12.6 binding site (amino acids 2361 -2496) within the central HD1 domain of RyR2 (Dhindwal et al., 2017; Laitinen et al., 2001; Lehnart et al., 2004; Marx et al., 2000; Xiao et al., 2016; Zissimopoulos and Lai, 2005). FKBP12 and FKBP12.6 are RyR2-associated proteins, reported to stabilise channel opening to the maximum conductance (Ahern et al., 1994; Brillantes et al., 1994; Lehnart et al., 2004; Marx et al., 2000; Wehrens et al., 2003). We find that FKBP12/12.6 removal from sheep RyR2 is correlated with increased sub-conductance activity in one RyR2 channelopathy linked to a mutation in the RyR2-associated regulatory protein, CLIC-2 (Richardson et al., 2017). While the RyR2-FKBP12/12.6 association is widely documented, its role in modulating RyR2 channel activity is disputed (Meli et al., 2011; Shan et al., 2010; Xiao et al., 2007; Zissimopoulos and Lai, 2005).

Taking these considerations together, the ion channel properties of P2328S RyR2 from the RyR2^{S/S} mouse model have wide reaching implications for cardiac dysfunction and physiology. We have examined the conductance and single channel parameters of RyR2 from WT and RyR2^{S/S} mice, their cytoplasmic Ca^{2+} -sensitivity, their FKBP12 association and S2814 and S2808 phosphorylation. We refer to FKBP12 rather than FKBP12.6 as we mainly saw only one FKBP band associated with RyR2 in mouse heart, where the ratio of FKBP12/FKBP12.6 associated with RyR2 is ~0.01 (Zissimopoulos et al., 2012). Overall, we find that neither the full conductance of the channel, nor its sub-conductance properties are altered by the mutation. Ca^{2+} activation and, surprisingly, Ca^{2+} -inactivation of mutant channels, are shifted to lower cytoplasmic $[\text{Ca}^{2+}]$ so that the channel is maximally activated between 100 nM and 1 μM Ca^{2+} . In contrast to channels expressed in HEK 293 cells, these changes are apparent without adrenergic stimulation and without loss of RyR2-associated FKBP12 or change in RyR2 S2814 or S2808 phosphorylation. The differences between the properties of channels expressed in mouse and in HEK 293 cells emphasise the importance of examining channels expressed in mature mammals.

Results.

Conductance of WT and P2328S RyR2 channels at 1mM and 1μM cytoplasmic [Ca²⁺].

In initial experiments (experiment #1), WT and P2328S RyR2 activity was recorded continuously following channel incorporation into bilayers, starting with solutions on either side of the bilayer containing 1 mM Ca²⁺. The cytoplasmic [Ca²⁺] was lowered after 3 to 5 minutes to 1 μM (Methods), a concentration that might exist in myocytes towards the end of diastole. There were no significant differences between the average maximum conductance of WT and P2328S channels recorded at the same bilayer voltage and cytoplasmic [Ca²⁺] (Figs 1A-1D). However, currents in both channel types were greater with 1 μM cytoplasmic Ca²⁺ than with 1 mM Ca²⁺, likely due to removal of partial pore block due to Ca²⁺ binding (Hanna et al., 2014; Friel and Tsien, 1989; Gillespie et al., 2005). There was a small but significantly greater conductance in WT channels at -40 mV (with current flow from lumen to cytoplasm) which is also observed in sheep RyR2 (Dulhunty – unpublished observations), and a similar trend in P2328S channels.

The activity of WT and P2328S RyR2 channels at 1 mM and 1 μM cytoplasmic Ca²⁺ and ATP sensitivity.

The biphasic cytoplasmic [Ca²⁺] - dependence of sheep and canine RyR2 channels shows a strong increase in activity between 1 μM and 10 μM Ca²⁺, a plateau between 10 μM and 1 mM and inactivation at concentrations $\gg 1$ mM (Laver et al., 1995; Xu and Meissner, 1998). Thus the decline in the activity of the mouse WT channel in Fig. 1A when cytoplasmic Ca²⁺ was lowered from 1 mM to 1 μM was expected. The activity of the P2328S channel was similar to that of the WT channel with 1 mM cytoplasmic Ca²⁺, but was markedly higher when the [Ca²⁺] was lowered to 1 μM. This difference is reflected in the open probability (P_o) of most individual channels (Fig. 2 and Figs S1, S3, S4: where lines connect data for individual channels at 1 mM and 1 μM Ca²⁺). Despite the usual (>10-fold) variability between P_o of individual channels (Copello et al., 1997) at both 1 mM and 1 μM cytoplasmic Ca²⁺, the open probability of each WT channel was substantially lower with 1 μM than 1 mM Ca²⁺ (Figs 2A,B). The P2328S channels were more variable, with activity dropping in 9 of 14 channels, changing very little in 2 channels or increasing in 3 channels. As in Fig. 1 above, a robust voltage-dependence of P_o in these mouse RyR2 channels is notable in Fig. 2 and Figs S1, S3, S4, with higher P_o at -40 than +40 mV in both WT and P2328S channels. The higher P_o at -40 mV suggests that the mutation would have the greatest impact when Ca²⁺ moves from the lumen of the SR into the cytoplasm, during systole and during diastolic Ca²⁺ leak. This voltage-dependence of P_o has been reported in sheep RyR2 (Dulhunty et al., 1999; Laver and Lamb, 1998; Sigalas et al., 2009), but is not apparent under all conditions (Dulhunty et al., 1999; Hewawasam et al., 2010; Laver and Lamb, 1998; Sigalas et al., 2009).

The P_o data in Fig. 2 is replotted on a logarithmic scale in Fig. S1 to show the spread of lower P_o values over an ~100-fold range with 1 μM cytoplasmic Ca²⁺ at +40 mV. This in most cases exceeds the ~10-fold range with 1 mM cytoplasmic Ca²⁺. The tighter range of values with 1 mM cytoplasmic Ca²⁺ may reflect more cohesive gating of P_o at maximally activated levels or a clustering due to the limiting P_o value of 1.00.

Parameter values from single and multiple RyR2 channels were included in the average P_o in Fig. 3A (assuming that I'_F for multiple channels is equal to the average P_o of the individual channels, Methods). The mean open time (T_o), mean closed time (T_c) and event frequency (F_o) could be measured only in single channel

recordings (Figs 3B, C, D). There were no significant differences between WT and P2328S in any of the average parameters with 1 mM Ca^{2+} . In marked contrast, with 1 μM Ca^{2+} the average P2328S P_o , T_o and T_c were significantly different from WT, with P2328S channels having higher P_o , longer openings and briefer closures. The higher WT P_o at 1 mM compared to 1 μM Ca^{2+} was due to significantly longer T_o , briefer T_c and higher F_o . Average P2328S P_o was also higher with 1 mM than 1 μM Ca^{2+} due to a significantly higher F_o and a trend towards longer open durations. The difference between P_o at 1 μM and 1 mM Ca^{2+} was substantially less in P2328S than in WT channels. Given the voltage-dependence of channel activity (Figs 1, 2 above), the gating parameters are plotted separately for -40 and +40 mV in Fig. S2. The difference between WT and P2328S P_o were significant at each potential, but the other parameters mainly showed trends in the same directions as the significant changes in the combined data (Fig. 3A-D).

Overall the results in Figs. 3A-D and S2 show that increases in WT channel P_o between 1 μM and 1 mM Ca^{2+} are due to cytoplasmic Ca^{2+} increasing the duration and frequency of channel openings, while reducing the closed times. There were smaller differences between 1 μM and 1 mM Ca^{2+} in P2328S RyR2, with the significant increases in P_o and F_o , and trends towards a longer T_o and shorter T_c . The reduced sensitivity to this change in $[\text{Ca}^{2+}]$ in P2328S RyR2 could be due to either a reduced cytoplasmic Ca^{2+} sensitivity or a shift in the cytoplasmic Ca^{2+} -dependence. These possibilities are explored in the following section.

Since the P2328 residue is contained within an RyR2 sequence that also binds ATP (Blayney et al., 2013), we examined the effect of the P2328S mutation on ATP activation. Cytoplasmic addition of 2 mM Na_2ATP caused an increase in P_o in all WT and P2328S channels examined and a significant increase in the average P_o of WT RyR2 in the presence of 1 μM Ca^{2+} and of P2328S channels in the presence of 1 μM and 100 nM cytoplasmic Ca^{2+} (Fig. 3E). In the presence of ATP, average P_o was significantly greater in P2328S with 1 μM Ca^{2+} than in WT channels or P2328S with 100 nM Ca^{2+} . Prior to ATP addition, P_o with 1 μM Ca^{2+} was significantly greater in P2328S than WT channels or P2328S channels with 100 nM Ca^{2+} . However, relative increases in P_o were the same in all cases (Fig. 3F), indicating that ATP-activation *per se* was unaffected by the P2328S mutation.

Redox buffering was addressed in a subset of 3 WT and 3 P2328S ATP-activated channels. The GSH:GSSG ratio was set to an oxidizing potential (see Methods) in cytoplasmic and luminal solutions to mimic cardiac oxidative stress (Oda et al., 2015). There was a trend towards the expected increase in P_o WT channels (Pessah et al., 2002). The average WT P_o (data at +40 and -40 mV pooled) was 0.086 ± 0.045 with ATP before, and 0.162 ± 0.108 after, redox buffering. P2328S P_o was 0.191 ± 0.078 before, and 0.163 ± 0.051 after redox buffering. Although incomplete, these results suggest that the mutant channels may be less sensitive to oxidizing cytoplasmic conditions than WT channels.

Cytoplasmic Ca^{2+} sensitivity of WT and P2328S RyR2 channels.

In experiment #2, the cytoplasmic incorporation solution containing 1 mM Ca^{2+} was replaced immediately after incorporation by perfusion with solutions containing 100 nM or 300 nM Ca^{2+} (Methods).

The $[Ca^{2+}]$ was then increased stepwise to 1 mM by addition of appropriate aliquots of $CaCl_2$. The P_o for WT channels at 1 mM and 1 μM (Fig. 4) were not significantly different from those obtained in the first experiment. However, in contrast to experiment #1, the activity of most P2328S channels in experiment #2 declined at the higher Ca^{2+} concentrations (see individual channels in Figs S3, S4). Average P2328S P_o was significantly less with 1 mM Ca^{2+} than at lower $[Ca^{2+}]$ s at +40 mV (Fig. 4D), while at -40 mV there was a trend towards a lower P_o at 1 mM than 1 μM Ca^{2+} (Fig. 4C).

The difference between the two experiments may have reflected the different order in which the solutions were changed, but more likely reflected differences between individual P2328S channels. P_o was lower with 1 μM Ca^{2+} than 1 mM Ca^{2+} in all WT channels. On the other hand, P2328S P_o in experiment #1 was greater or no different with 1 μM than 1 mM Ca^{2+} in 3 of 11 channels, while in experiment #2 P_o was greater or no different in 7 of 8 channels. Taking the two experiments together, the activity of 10 of 19 P2328S channels was lower with 1 mM Ca^{2+} than with 1 μM Ca^{2+} .

The average P_o values for WT channels described classical Ca^{2+} -activation curves for RyR2 with P_o increasing steeply between 1 μM and 10 μM Ca^{2+} and reaching a plateau between 10 μM and 1 mM Ca^{2+} (Fig. 4A,B). Inactivation is not apparent in the WT data as it occurs when the cytoplasmic $[Ca^{2+}]$ is increased to non-physiological levels >1 mM (Laver et al., 1995). The Ca^{2+} -dependence of P_o was substantially altered by the RyR2-P2328S mutation (Fig. 4C,D). The increase in P2328S RyR2 P_o with Ca^{2+} -activation was shifted to lower $[Ca^{2+}]$ s, with a maximum at 1 μM Ca^{2+} (-40 mV) or ~ 300 nM (+40 mV). The average P_o declined with further increases in $[Ca^{2+}]$, likely reflecting Ca^{2+} -dependent inactivation and suggesting an unexpected shift in the inactivation curve into the physiological range of cytoplasmic $[Ca^{2+}]$.

Hill equations for Ca^{2+} -dependent activation and inactivation (Methods) were fitted to the data in Fig. 4. Affinity constants for activation and inactivation (K_A and K_I respectively) and Hill coefficients for activation and inhibition (H_A and H_I respectively) for the fitted curves are listed in Table 1. The P2328S mutation caused an ~ 10 -fold shift in Ca^{2+} -activation. The affinity constant decreased from WT values of 3.5 μM to 0.32 μM Ca^{2+} in mutant channels at -40 mV, and from 1.5 μM in WT to 0.15 μM Ca^{2+} in mutant channels at +40 mV. Inactivation for P2328S RyR2 channels was shifted ~ 1000 fold from mM levels in WT channels to 7 μM at +40 mV or 1 μM at -40 mV. Additionally, the P2328S RyR2 inactivation curve at +40 mV ($K_I = 1.0$ μM) overlapped the activation curve ($K_A = 0.15$ μM). Therefore, the maximum P_o achieved of 0.35 was less than the maximum of 0.52 if activation had proceeded in the absence of inactivation. This is the first report of a RyR2 mutation causing such a dramatic shift in the Ca^{2+} -dependence of inactivation. In contrast to the marked changes in K_i and K_A , there was no change in the Hill coefficients, indicating that, as expected, the number of binding sites does not change.

The best fit of the Hill equations to the data required two assumptions. Firstly that there is a baseline P_o (BP_A) at $[Ca^{2+}]$ s less than activating levels, of 0.02 for WT RyR2 at -40 mV or 0.014 at +40 mV, or for P2328S of 0.1 at -40 mV or 0.05 at +40 mV. Secondly, that inactivation in P2328S RyR2 reduced P_o to a baseline level (BP_I) of 0.26 at -40 mV or 0.11 at +40 mV, that was higher than the WT channels BP_I of 0.05 at -40 mV and or 0.055 at +40 mV.

Sub-conductance activity in WT and P2328S RyR2 channels.

Given the reported associations between arrhythmogenic mutations in RyR2, sub-conductance activity, phosphorylation and amounts of FKBP12 associated with RyR2 (Introduction), we examined sub-conductance levels, FKBP12 binding to, and phosphorylation of, WT and P2328S RyR2 channels. Strong sub-conductance opening to current levels less than the maximum single channel current was apparent in both channel types and is apparent in selected segments of activity from 24 different channels in Fig. 5 (with 1 mM cytoplasmic Ca^{2+}) and Fig. 6 (with 1 μM cytoplasmic Ca^{2+}). There were no consistent differences between the WT and P2328S RyR2 channels in sub-conductance levels or in amounts of sub-conductance activity. In each case there are brief and very long openings to levels between 25% and 75% of the maximum current, with multiple levels as well as one or two dominant levels. The same lack of difference is apparent in the longer recordings from 18 WT and 18 P2328S channels in Figs S3,S4. Sub-conductance levels were generally scaled to the maximum current, so that the intervals between levels was least with 1 mM cytoplasmic Ca^{2+} and +40 mV. Channel openings in WT and P2328S RyR2 are generally more clearly defined at -40 mV with 1 μM Ca^{2+} (Fig. 6) than 1 mM cytoplasmic Ca^{2+} (Fig. 5). The lack of differences between the sub-conductance activity was not due to selection of the current segments in Figs 5, 6 as they are clearly seen in the longer records of continuous activity from a larger number of channels shown in Figs S3,S4. No quantitative evaluation of sub-conductance levels was attempted as we concluded that the activity was not substantially altered by the P2328S mutation.

FKBP12 and 12.6 association with WT and P2328S RyR2 channels.

FK506 binding protein associated with the RyR2 was examined in the context of two controversial questions. Firstly, the correlation between sub-conductance activity and FKBP bound to RyR2 (Galfré et al., 2012; Lam et al., 1995) and secondly whether the binding of FKBP to RyR2 is generally altered as a result of disease-associated mutations in RyR2 (Lehnart et al., 2004; Meli et al., 2011) or heart failure (Marx and Marks, 2002). Consistent with reported amounts of FKBP12.6 associated with RyR2 in mouse heart being ~100-fold lower than FKBP12 (Zissimopoulos et al., 2012), we failed to see any convincing band corresponding to FKBP12.6 in Western blots of WT or P2328S RyR2 mouse hearts. We routinely see bands corresponding to both isoforms in Western blots of sheep and human heart (Richardson et al., 2017; Walweel et al., 2017). Blots of FKBP12 associated with RyR2 in SR vesicles suggest that there is no difference between WT or P2328S RyR2 (Fig. 7A) and there was no significant difference between the average associated amounts (Fig. 7B).

Phosphorylation of WT and P2328S RyR2 channels

Hyperphosphorylation of RyR2 at S2808 and S2814 is associated with ventricular arrhythmia and FKBP dissociation from RyR2 (Dobrev and Wehrens, 2014). S2808 is hyperphosphorylated in humans and dogs with chronic AF (Vest et al., 2005). Human and rat S2804 and/or S2814 are basally phosphorylated and hyperphosphorylated after β -adrenergic stimulation (Denniss et al., 2018; Li et al., 2013; Walweel et al., 2017). Phosphorylation of RyR2 S2804 and S2814 in SR vesicles from WT and RyR2^{S/S} mouse hearts was immuno-detected in Western blots using antibodies that specifically recognise those residues only when they

are phosphorylated. Both residues are basally phosphorylated in the absence of any experimental adrenergic treatment and there was no difference between the basal phosphorylation in WT or P2328S RyR2 in the individual blots (Fig. 7C, E) or in the average normalised data (Fig. 7D, F).

Discussion

Our findings demonstrate that mouse RyR2-P2328S (P2328S) channels are more active than WT RyR2 channels over the lower spectrum of physiologically relevant cytoplasmic Ca^{2+} concentrations (0.1 – 1 μM), with both Ca^{2+} activation and inactivation shifted respectively to nanomolar or micromolar Ca^{2+} . Notably this change in Ca^{2+} -sensitivity occurred in the absence of adrenergic challenge. The channel properties indicate that P2328S RyR2 activity may be close to a balance between controlled and uncontrolled Ca^{2+} leak prior to adrenoceptor activation and that such a challenge could tip the balance and trigger the cascade of events leading to potentiation of aberrant diastolic Ca^{2+} release. The greatly altered channel characteristics occurred without alterations in maximum conductance or subconductance activity and without change of FKBP12 binding or RyR2 S2808/S2814 hyperphosphorylation, again in the absence of adrenergic challenge. This suggests a mechanism for enhanced channel activity in P2328S-associated CPVT that does not depend on hyperphosphorylation or loss of FKBP12/12.6-mediated stabilisation of RyR2 channels. Notably our findings parallel cellular evidence that cardiomyocytes from RyR2^{S/S} hearts have higher incidences of spontaneous diastolic events than WT hearts without adrenergic challenge (Goddard et al, 2008; Zhang et al., 2011).

Channel activity and its Ca^{2+} dependence in murine WT and P2328S RyR2 channels

The significantly higher P_o at 1 mM compared with 1 μM cytoplasmic Ca^{2+} in mouse WT RyR2 was similar to that in sheep and canine RyR2 (Sitsapasan and Williams, 1994; Xu and Meissner, 1998). The P2328S mutation blunted this difference between P_o at 1 μM and 1 mM Ca^{2+} (experiment #1) so that P2328S RyR2 channels were more active than WT RyR2 at 1 μM cytoplasmic Ca^{2+} (Figs 1, 2, 3). Activity in both channel types was significantly greater with current flow from lumen to cytosol at -40 mV.

The higher activity in P2328S RyR2 channels at 1 μM Ca^{2+} was due to a strong leftward shift to activation at lower $[\text{Ca}^{2+}]$, such that the channels were between 30% to 50% activated by 100 nM Ca^{2+} and fully activated with 1 μM Ca^{2+} . This would lead to pronounced diastolic Ca^{2+} leak through P2328S channels that would be expected to be strongly pro-arrhythmic. A leftward shift in the Ca^{2+} activation curve is common with CPVT mutations (Meli et al., 2011; Xiao et al., 2016) and not surprising. However, the stronger ~1000-fold shift in Ca^{2+} -inactivation is a novel finding. This inactivation within the normal range of systolic $[\text{Ca}^{2+}]$ could truncate systolic Ca^{2+} release, thus reducing contraction. However, we predict that systolic Ca^{2+} release may not be affected, because the weaker shift in inactivation at -40 mV (current flow from lumen to cytoplasm) meant that P_o at -40 mV was similar in WT and P2328S channels at peak Ca^{2+} transient levels around 10-15 μM Ca^{2+} . Consistent with this prediction, there are no reports suggesting reduced contraction with RyR2-

P2328S mutations in humans or in the mouse model, while systolic Ca^{2+} transient amplitudes are similar in cardiomyocytes from WT and RyR2^{S/S} mice (Goddard et al, 2008; Zhang et al., 2011).

To fit Hill equations to the data, we assumed finite baseline activity levels. The baseline P_o at $[\text{Ca}^{2+}]$ below activation was higher in P2328S than WT channels at -40 mV and with Ca^{2+} -inactivation, P2328S P_o decayed to a baseline level greater than the level before Ca^{2+} -activation (Table 1), suggesting incomplete inactivation. The magnitude of the baseline P_o reported here would lead to massive diastolic Ca^{2+} leak. This would be less in myocytes where other factors including Mg^{2+} modulate channel activity. The effect of Mg^{2+} was not addressed in bilayer experiments because, in the absence of ATP and with cytoplasmic $\text{Ca}^{2+} \leq 1 \mu\text{M}$, Mg^{2+} effectively reduces WT channel activity to such low values that quantification of channel activity is unreliable (Laver et al., 1997a; Xu et al., 1996). Never-the-less we predict that even a smaller increase in baseline activity with the P2328S mutation would contribute significantly to increased diastolic Ca^{2+} leak.

The impact of ATP-activation and potential Mg^{2+} -inhibition on P2328S channels.

The ATP binding site involves RyR1 residues M4954 and F4959 at the C-terminus of transmembrane S6 helix (des Georges et al., 2016). Equivalent RyR2 residues, M4884 and F4889, are presumably also adjacent to S6. P2328 is situated in the HD1 helical domain which interacts extensively with regions near the ATP binding site (Dhindwal et al., 2017). Indeed, Blayney et al (2013) found high affinity ATP binding to the G2236-G2491 fragment (encompassing HD1, HD2 and P2328) (Blayney et al., 2013). That we did not see an effect of P2328S on ATP-activation suggests that the P2328 residue is not involved in ATP binding. Similar ATP scaling of WT and P2328S activity suggests that the Ca^{2+} -dependence of activation and inactivation may not be altered by ATP, although P_o would be higher.

The effects of the P2328S mutation on cytoplasmic Mg^{2+} - and luminal Ca^{2+} -and Mg^{2+} -sensitivity, or other regulatory factors like H^+ , calmodulin, oxidation and nitrosylation were beyond the scope of this study. However it is interesting that Lehnart et al (2004) found a right shift in cytoplasmic “ Mg^{2+} -inhibition” of P2328S channels which may appear inconsistent with the left shift we see in Ca^{2+} inactivation as cytoplasmic Mg^{2+} of ~1 mM can occupy the Ca^{2+} inactivation site and inhibit RyR2. However, Mg^{2+} can bind to two independent cytoplasmic Ca^{2+} binding sites on RyR2, with effects that depend on cytoplasmic $[\text{Ca}^{2+}]$. The low-affinity inhibitory (II) site does not discriminate between Ca^{2+} and Mg^{2+} and Mg^{2+} binding to this site leads to Mg^{2+} -inhibition with $\geq 100 \mu\text{M}$ cytoplasmic $[\text{Ca}^{2+}]$ (Laver, 2010; Walweel et al., 2014). This would indeed parallel the Ca^{2+} -inactivation that we describe here. Mg^{2+} also binds to the higher affinity Ca^{2+} activation (A-) site, which selects Ca^{2+} over Mg^{2+} by ~50-fold (Laver, 2010). 1 mM Mg^{2+} binds to the A-site and prevents Ca^{2+} in low μM range from binding and activating RyR2 (Laver, 2010), i.e. it prevents Ca^{2+} activation rather than inhibiting the channel. The “ Mg^{2+} -inhibition” described by Lehnart et al (2004) using 150 nM cytoplasmic Ca^{2+} likely reflects Mg^{2+} binding to the A-site. A right shift in “ Mg^{2+} -inhibition” at the A-site in P2328S RyR2 is consistent with reduced Mg^{2+} binding as a result of enhanced Ca^{2+} affinity, allowing activation by 150 nM Ca^{2+} . The relief of A-site Mg^{2+} binding would further enhance Ca^{2+} leak during diastole. |

Lack of alterations in FKBP association or phosphorylation in mouse P2328S RyR2 channels

The significant changes in the Ca^{2+} -activation curve in mouse P2328S channels did not depend on adrenergic challenge, unlike P2328S channels expressed in HEK 293 cells where increased activity with 150 nM Ca^{2+} was seen only after protein kinase A phosphorylation (Lehnart et al., 2004). Our observations are more consistent with those of Zhang et al. (Zhang et al., 2011) who found significantly higher incidences of arrhythmia in isolated perfused RyR2^{S/S} hearts, compared to WT, prior to adding isoproterenol. In addition, diastolic Ca^{2+} release events are seen in isolated RyR2^{S/S}, but not RyR2^{+S} or WT atrial myocytes in the absence of isoproterenol (Goddard et al. 2008; Zhang et al. 2011). The difference between results with RyR2 P2328S channels expressed in HEK 293 cells and those with adult mice may not be surprising given that native channels from mouse are associated with regulatory proteins including triadin, junction and calsequestrin that are lacking in the recombinant system. These contrasts underline the importance of examining the effects of mutations on RyR2 channels expressed in adult mammalian tissue.

The correlation between leaky RyR2 channels carrying CPVT mutations and FKBP binding to the channels is controversial. Reduced FKBP12.6 binding to recombinant RyR2 channels is reported with P2328S, S2226L, R2474S and R4497C CPVT mutations (Lehnart et al., 2008; Wehrens et al., 2003) and increasing FKBP12.6 association with RyR2 can prevent aberrant SR Ca^{2+} release with AF and CPVT (Meli et al., 2011; Shan et al., 2012; Wehrens et al., 2003). Conversely, the CPVT R2474S RyR2 demonstrated increased FKBP12.6 affinity (Tiso et al., 2002), while enhanced FKBP12.6 binding did not alter arrhythmias in R4496C mice (Liu et al., 2006).

A complication with evaluating reported FKBP interactions with RyR2 was the assumption that RyR2 associates with FKBP12.6 alone, as FKBP12.6 was discovered in heart (Timerman et al., 1996). Therefore, many studies assumed that any FKBP bound to RyR2 was FKBP12.6, and only FKBP12.6 has been added to RyR2 in numerous functional studies. However many mammalian species (mouse, pig and rabbit), have more FKBP12 associated with RyR2 than FKBP12.6 (Zissimopoulos et al., 2012). A further complication is that FKBP12 and FKBP12.6 have different actions on RyR2: FKBP12 being a high affinity sheep RyR2 activator, whereas FKBP12.6 has low efficacy, but antagonises the effects of FKBP12 (Galfré et al., 2012). There are no similar comparative reports for human or mouse RyR2. However we find robust amounts of FKBP12 bound to healthy human (Walweel et al., 2017) and mouse RyR2 (Fig. 7). It may be more relevant to examine FKBP12 rather than, or combined with, FKBP12.6, association with RyR2 channels.

Altered subconductance opening has been attributed to altered FKBP12/12.6 binding to RyR2 (Lehnart et al., 2004; Marx et al., 2000; Richardson et al., 2017; Wehrens et al., 2003) or FKBP12 binding to RyR1 (Ahern et al., 1994; Brillantes et al., 1994). Our observations that neither the amount of FKBP12 bound to RyR2 nor subconductance activity are altered by the P2328S mutation again indicate a correlation between these parameters. That FKBP12 was not dissociated from P2328S RyR2 is consistent with a mutation in the HD1 domain (Dhindwal, 2017) which is distant from FKBP12 binding sites within RyR2 305-784 and 1815-1855 (Meli et al., 2011; Xiao et al., 2016) in both the linear sequence and 3D structure. Although FKBP12.6 stabilises HD2 (2982-3528), it does not alter HD1 (2110-2679) structure (Dhindwal, 2017).

As neither FKBP12 nor phosphorylation are significant in the RyR2^{S/S} model, ‘intramolecular domain unzipping’ may lead to CPVT in RyR2 P2328S carriers. Interactions between N-terminal and central domains stabilise the channel closed state (Liu and Priori, 2007; Marks, 2002). As P2328S lies within the leucine rich HD1 region (Dhindwal, 2017), the mutation could cause unzipping, hence decreasing the ability of the channel to remain closed and rendering it more sensitive to changes in cytosolic Ca²⁺ (Priori and Chen, 2011; Sumitomo, 2016), independent of FKBP12/12.6 or phosphorylation (Oda et al., 2015). Consistently, closed times here were significantly shorter in P2328S channels. Since our findings are in the absence of adrenergic activation, the changes could be more extreme during adrenergic stimulation, which increases channel activity at diastolic cytoplasmic [Ca²⁺] primarily through effects on luminal Ca²⁺- and Mg²⁺-regulation without altering A-site Ca²⁺ or Mg²⁺ regulation (Li et al., 2013). Provided the mutation did not alter the influence of phosphorylation on these luminal sites, we predict that adrenergic stimulation would further enhance channel activity at diastolic [Ca²⁺].

The impact of changes in P2328S channel activity on Ca²⁺ efflux from the SR during diastole, DAD generation and arrhythmia.

It is significant that, with diastolic cytoplasmic Ca²⁺ levels between 300 nM and 1 μM, P_o is 3 to 5 times greater in P2328S than WT channels. At 1 μM cytoplasmic Ca²⁺, P2328S channel P_o is similar to the maximum Ca²⁺-activated P_o of WT channels with >10 μM cytoplasmic Ca²⁺. Therefore, robust local Ca²⁺ release from the RyR2^{S/S} mouse SR during diastole could lead to Ca²⁺ waves. Indeed, we previously reported ectopic Ca²⁺ transients in regularly stimulated RyR2^{S/S} murine hearts without adrenergic challenge, but not in their WT counterparts (Goddard et al., 2008). It is estimated that release of 30 to 40 μM of Ca²⁺ would be required to depolarize myocyte membranes to action potential threshold (Schlotthauer and Bers, 2000). Several factors may contribute to preventing this release from triggering an action potential in normal myocytes, providing a 3- to 4-fold safety margin (Schlotthauer and Bers, 2000). The 3 to 5 times greater activity of P2328S RyR2 channels during diastole could overcome this safety margin, allowing greater local increase in cytoplasmic [Ca²⁺] and stronger depolarization, triggering action potentials. It is likely that subclinical arrhythmic events such as ectopic action potentials or non-sustained VT occur without harming individuals and therefore remain undetected. Indeed, this may occur more frequently than anticipated as more severe arrhythmic events, including polymorphic VT and sudden cardiac death, occur in CPVT patients at rest and during sleep (Allouis et al., 2005; D’Amati et al., 2005; Goddard et al., 2008; Postma et al., 2005). The incidence of severe arrhythmic events may be further increased by even relatively mild adrenergic challenge.

General characteristics of single mouse WT and P2328S RyR2 channels

Single channel analysis revealed some fundamental properties common to WT and P2328S RyR2 channels which have not been reported, or which have been relatively overlooked in recent literature. 1). Channel conductance is significantly greater in WT channels when current flow is from lumen to cytoplasm (-40 mV), as during systole or diastolic “leak”, with a similar trend in P2328S channels. 2). Millimolar cytoplasmic Ca²⁺ lowers channel conductance, due to Ca²⁺ blocking the pore (Hanna et al., 2014; Friel and Tsien, 1989; Gillespie et al., 2005). 3). P_o is highest when current flow is from the lumen to the cytoplasm.

This has been attributed to “feed through activation” whereby luminal Ca^{2+} flows through the channel and binds to cytoplasmic Ca^{2+} -activation sites (Sitsapesan and Williams, 1994; Tripathy and Meissner, 1996); or to Ca^{2+} binding to luminal Ca^{2+} activation sites (Laver, 2007). We see a greater P_o at -40 mV when both cytoplasmic and luminal solutions contain 1 mM Ca^{2+} , so that both cytoplasmic and luminal Ca^{2+} activation sites would be occupied. Therefore, our results suggest that there is indeed a voltage, or direction of current flow sensor, within the transmembrane domain of the RyR2 that regulates channel gating and is not influenced by the P2328S mutation. The overall significance of this sensor would be to amplify channel activation by Ca^{2+} induced Ca^{2+} release during systole and during diastolic leak, particularly with the excess Ca^{2+} release imposed on the channel by the P2328S mutation.

Finally our results demonstrate the well-documented (Copello et al., 1997) spread in parameter values in individual WT channels, which is exacerbated in P2328S channels as it is in human heart failure (Walweel et al., 2017). In experiment #1 (1 μM cytoplasmic Ca^{2+} at -40 mV), the range of WT P_o was 0.0016 to 0.11, compared to 0.0027 to 0.875 in P2328S channels. The WT variability is likely a consequence of the size of the RyR2 protein and number of regulatory sites, which may be vacated or occupied on each of the four subunits to different extents in each functional ion channel. Added to this, the increased P2328S variability was partly due to P_o remaining unchanged or increasing in many P2328S channels when cytoplasmic Ca^{2+} was reduced from 1 mM to 1 μM , in contrast to WT channels where P_o fell to lower values in all cases. A consequence of the variability is that although changes in average gating parameters are often not significant, trends are indicative of underlying gating changes.

Concluding comments

P2328S channels show increased sensitivity to cytosolic Ca^{2+} in the absence of adrenergic challenge. This could contribute significantly to the potentiation of aberrant SR Ca^{2+} leak under resting conditions thus triggering cardiac arrhythmias and sudden cardiac death. The increase in open probability was observed in the absence of altered levels of FKBP12 binding or phosphorylation. This is contrary to findings with FKBP12.6 and phosphorylation with the same mutation and also some other mutations in RyR2 channels expressed in a HEK cell system, albeit following PKA stimulation (Wehrens et al., 2003; Lehnart et al., 2004; Meli et al., 2011). We uncovered a novel leftward shift in Ca^{2+} -dependent inactivation towards the range of $[\text{Ca}^{2+}]$ achieved during systole, with incomplete inactivation. While this might not impact on the peak systolic Ca^{2+} transient, incomplete inactivation would contribute to maintaining cytoplasmic Ca^{2+} at a higher than normal level during diastole and add to the potential for DADs and arrhythmia. Overall, our results are consistent with the increased sensitivity to cytosolic Ca^{2+} suggested in RyR2^{S/S} mouse cells (Goddard et al. 2008; Zhang et al. 2011). It is worth considering the location of P2328 and its proximity to Ca^{2+} -activation and inactivation sites in the high resolution structure of the RyR. The cytoplasmic Ca^{2+} and Mg^{2+} A- and ATP-binding sites are located near the transmembrane channel pore region (des Georges et al., 2016; Jones et al., 2017) that interacts with HD1 residues containing P2328 (Dhindwal et al., 2017). A predicted Ca^{2+} and Mg^{2+} II-binding site in residues 1873–1903 is located in the handle domain of RyR1 (Laver, 2018; Laver et al., 1997b), close in space to the HD domains (Yan et al., 2015). Therefore, structural changes in the HD1 domain caused by the P2328S

mutation could sterically influence both the A and I1 Ca²⁺-binding sites producing the changes in channel activity reported here.

Materials and Methods

Harvesting of mouse hearts:

WT and homozygous *RyR2-P2328S* inbred 129/Sv mice, age matched across 3 – 7 months (in order to obtain a range that would represent a similar magnitude of age distribution in the human population), were killed by cervical dislocation in licensed institutional premises under the UK Animals (Scientific Procedures) Act 1986. Homozygous mice were used to ensure that all RyR2 channels were P2328S homotetramers and to reveal the full extent of the effect of the mutation. The hearts were rapidly excised and transferred to ice cold Krebs-Henseleit buffer (in mM: NaCl 119, NaHCO₃ 25, KCl 4, KH₂PO₄ 1.2, MgCl₂ 1, CaCl₂ 1.8, glucose 10 and Na-pyruvate 2; pH 7.4, 95% O₂/5% CO₂) to rinse and remove excess tissue and blood. The whole heart was then snap frozen in liquid N₂. Hearts were couriered to Australia on dry ice and then stored at -80°C.

Isolation of the RyR2 SR vesicle preparation:

All steps of the SR vesicle preparation were performed on ice and/or at 4°C. For lipid bilayer experiments, 5 to 7 hearts were homogenised in cardiac homogenising buffer (CHB, containing mM: Sucrose 290, imidazole 10, and NaN₃ 3, pH 6.9). The homogenate was then centrifuged at 12,000 x g for 20 min, then the pellet discarded and the supernatant centrifuged at 43,000 x g for 2 h. The pellet was resuspended in Buffer A (CHB plus 649 mM KCl) and centrifuged at 46,000 x g for 1.5 h. This pellet was re-suspended in 125 µl per gm of mouse hearts (~5 hearts) of buffer A plus protease inhibitor mixture and stored in 8 µl aliquots at -80°C for use in lipid bilayer experiments. All individual protease inhibitors were obtained from Sigma Aldrich and were added to the final suspension at the following final concentrations: Benzamidine hydrochloride hydrate – catalogue # B6506 – 1.0 mM; Pepstatin A – catalogue # P4265 – 2.1 µM; Leupeptin – catalogue # L2884 – 1 µM; AEBSF/Pefabloc SC – Catalogue # 76307 – 0.5 mM; Calpain Inhibitor I – catalogue # A6185 – 3 µM; Calpain Inhibitor II – Catalogue no. A6060 - 3µM.

Single channel lipid bilayer recordings:

Lipid bilayers were formed as previously described (Laver et al., 1995), by spreading a lipid mixture (phosphatidylethanolamine, phosphatidylserine and phosphatidylcholine in n-decane) across a 100 µm aperture in a partition separating the *cis* chamber from the *trans* chamber. SR vesicles were added to the *cis* solution so that, following incorporation, the cytoplasmic surface of SR and RyR2 faced that solution, which was then equivalent to the cytoplasmic solution. SR vesicles were incorporated using a cytoplasmic (*cis*) incorporation solution containing 230 mM caesium methanesulfonate (CsMS), 20 mM CsCl, 1 mM CaCl₂ and

10 mM tetraethylsulfamide (TES) pH 7.4, and a luminal (*trans*) solution containing 30 mM CsMS, 20 mM CsCl, 1 mM CaCl₂ and 10 mM TES pH 7.4. Following channel incorporation CsMS was added to the *trans* side to equalise the concentration of the charge carrier, [Cs⁺], in both solutions. Continuous current recording began at this point and continued for the duration of the experiment. A *cis* solution containing physiological cytoplasmic Ca²⁺ concentrations of 100 nM, 300 nM or 1 μM (with all other components identical to 1 mM Ca²⁺ *cis* solution) was introduced by a back-to-back 10 ml syringe aspiration-perfusion system designed to effectively replace the entire *cis* bathing solution. The Ca²⁺ concentration in the *cis* solution was later increased by adding appropriate amounts of CaCl₂, which were again determined using a Ca²⁺ electrode. In addition, in many channels after increasing [Ca²⁺] stepwise from 100 or 300 nM to 1 μM, 10 μM, 100 μM and 1 mM, we then re-perfused the *cis* chambers with the 100 or 300 nM Ca²⁺ solution and increased Ca²⁺ again to 1 μM or 10 μM. This allowed us to bracket at least some of the measurement and have more confidence in the results obtained for individual channels at lower [Ca²⁺]. All experiments were performed at a room temperature of 19 ± 1 °C.

Note that the *trans* (luminal) [Ca²⁺] was maintained at its physiological level of 1 mM throughout. Note also that the initial cytoplasmic [Ca²⁺] of 1 mM used for vesicle incorporation was higher than the cellular range of 100 nM-10 μM, but was required to facilitate channel incorporation. Measurement of channel activity with 1 mM cytoplasmic Ca²⁺ was nevertheless of considerable interest because it provided an indication of whether the plateau of RyR2 Ca²⁺-activation was maintained up to that concentration or whether activity declined due to the lower affinity Ca²⁺-inactivation process.

In some channels the redox potential of the cytoplasmic and luminal solutions was clamped to an oxidizing level of -180 mV by adding GSH/GSSG in the ratio of 0.95 mM/0.1 mM to each solution (Feng et al., 2000; Pessah et al., 2002), in the presence of cytoplasmic 1 μM Ca²⁺ and 2 mM ATP²⁻.

Single channel lipid bilayer electrophysiology and analysis.

Electrodes in the solutions on either side of the bilayer were used to voltage clamp the bilayer potential to -40 or +40 mV ($V_{cis} - V_{trans}$) and to detect current flow through the channel. Bilayer potential was switched between -40 mV and +40 mV every 30 s. The open probability (P_o), mean open time (T_o), mean closed time (T_c) were measured and subconductance activity analysed over 60 to 90 s of recordings in which only one channel opened in the bilayer, using the programs Channel 2 (developed by PW Gage and M Smith, JCSMR) or Channel 3 (developed by NW Laver, University of Newcastle). Channel 3 software can be obtained from Professor DR Laver (University of Newcastle, Newcastle, NSW, Australia). Threshold levels for channel opening were set to exclude baseline noise at ~20% of the maximum single channel conductance. P_o alone was evaluated in recordings containing more than one channel from the mean current divided by the maximum open current to obtain a value for the fractional mean current ($I'F$), which reflects P_o and is equal to P_o under ideal conditions.

A curve describing the changes in P_o with Ca²⁺ concentration was constructed by multiplying Hill equations for activation and inhibition (equations 1 and 2 respectively) which were modified from (Laver et

al., 1995) to include non-zero P_o values as indicated before Ca^{2+} activation (BP_A) and after Ca^{2+} -dependent inhibition BP_I , that were required to best fit the equations to the data.

$$P_o = BP_A + \frac{(P_o \text{ max} - BP_A)}{1 + \left(\frac{K_A}{[Ca^{2+}]}\right)^{H_A}} \quad \text{Eqn. 1, activation}$$

$$P_o = 1 - \frac{\left(1 - \left(\frac{BP_I}{P_o \text{ max}}\right)\right)}{1 + \left(\frac{K_I}{[Ca^{2+}]}\right)^{H_I}} \quad \text{Eqn. 2, inhibition}$$

$P_{o\text{max}}$ is the P_o of the maximally Ca^{2+} -activated channel, K_A and K_I are the Ca^{2+} affinities of the activation and inhibition sites.

Co-IP

Anti-RyR2 co-immunoprecipitation (Co-IP) of RyR2 complexes was performed to assess levels of FKBP12.0 and FKBP12.6 bound to RyR2 using the Pierce Co-IP kit and anti-RyR2 C3-33 antibody, following the manufacturer instructions (Walweel et al., 2017). In brief, 100 μg of SR were diluted to 1 $\mu\text{g}/\mu\text{l}$ in IP buffer (20 mM MOPS, 150 mM NaCl, 1 mM CaCl_2 , 1 X cOmplete, EDTA-free protease inhibitor cocktail ; pH 7.4) with 5% glycerol/0.1% Triton X-100, for 15 min on ice. Diluted SR samples were precleared with non-activated resin for 30 min at room temperature, with rotation. Precleared SR vesicles were separated from non-activated resin by centrifugation (1 min, 1000 x g), and incubated for 15 h at 4 °C (with rotation) with anti-RyR antibody-bound resin in IP buffer. Unbound protein was removed by 5 x washes of the complex with 200 μl of IP buffer, prior to elution of the anti-RyR2-RyR2 bound co-immunoprecipitate with 35 μl of 1 x LDL sample buffer with reducing agent at 60°C for 10 min. Samples were then subject to SDS Page and Western Blot (below).

SDS Page and Western Blot

SR vesicles (1-4 μg , for phosphor-protein detection) or co-immunoprecipitates (for FKBP and RyR2 detection), were subject to SDS Page and Western Blot according to (Laemmli, 1970; Towbin et al., 1979). Briefly, proteins were denatured in 1 x Bolt LSL sample buffer with reducing agent (Life Technologies) at 60 °C for 10min. Samples and standards were loaded onto a 4-15 % BOLT SDS polyacrylamide gel (ThermoFisher Scientific, Scorsby, Australia) and separated via electrophoresis using a Bolt Mini Gel system (ThermoFisher Scientific, Scorsby, Australia) at 165 V until the dye from reached the bottom on the gel. The gel was transferred to PVDF membrane within a Bio-Rad Mini-Protean Tetra cell (Bio-rad, Gladesville, Australia) in cold (4°C) transfer buffer (37 mM Tris, 140mM glycine, 20% ethanol, no pH adjustment). To maximize transfer of large molecular weight proteins (such as RyR2), the transfer was carried out 1 h at 100 mV, and then for an additional 30 min at 200 mV. PVDF membrane was blocked for 1-2 h at room temperature in blocking solution (3% BSA in PBS), and incubated with primary antibody (in PBS with 0.05% tween buffer)

overnight at 4 °C. Membranes were washed in PBS with 0.05% tween (5x), and incubated in appropriate secondary HRP-conjugated antibodies (IgG); in PBS with 0.05% tween) for 1.5-2 h at room temperature. Blots were washed 5 x in PBS+0.05% tween, once in PBS, prior to chemiluminescence detection.

Primary antibodies used were anti-RyR2 C3-33 (MA3-916 Ryanodine Receptor Monoclonal Antibody (C3-33), used at a concentration of 1 µg/mL (ThermoFisher Scientific, Scorseby, Australia)), anti-FKBP12 H5 (SC-133067 FKBP12 (H-5) mouse monoclonal antibody), used at a 1:200 dilution), (detects both 12.0 and 12.6 isoforms of FKBP, from Santa Cruz Biotechnology (Dallas, US)) and RyR2 pSer28084 (A010-30AP Ryanodine receptor 2 (RYR2) (pSer2808) rabbit polyclonal antibody, used at a 1:2000 dilution) and RyR2 pSer2814 (A010-31AP Ryanodine receptor 2 (RYR2) (pSer2814) rabbit polyclonal antibody. Used at a 1:5000 dilution), which detect the phosphorylated form of RyR2 residues S2808 or S2814, respectively, (Badrilla, Leeds, UK). The specificity of the pSer2814 and pSer2814 antibodies for phosphorylated S2808 and S2814 (respectively) was validated by maximally phosphorylating (with PKA and CamKII) and dephosphorylating (with PP1) RyR2, as previously described (Walweel et al., 2017). Specificity of anti-RyR2 C3-33 for RyR2 was validated by probing native RyR2 (in SR vesicles) and purified mouse RyR2.

Statistics

Average data is presented as mean±s.e.m. The significance of difference between various channel parameters for all channel data was assessed with 1- or 2-sided Student's T-test as appropriate. The significance of differences in the Co-IP and phosphorylation data were evaluated using ANOVA with Tukey post hoc testing. Differences were considered significant with $P < 0.05$.

Acknowledgements

The authors are grateful to Ms Suzy Pace and Ms Joan Stivala for their assistance with preparation of SR vesicles and general laboratory duties and to Dr Hermia Willemse for assistance with some channel and co-IP work.

Competing interests

No competing interests declared for, Esther M. Gallant, Nicole A. Beard; Angela F. Dulhunty; Samantha C. Salvage; Shiraz Ahmad, Haseeb Valli, James A. Fraser; Christopher L. Huang.

Funding

The work was supported by grants to AFD and NAB from the Australian National Health and Medical Research Council [APP108477 to A.F.D., APP1021342 to N.A.B and A.F.D.], to CLHH from the Medical Research Council (MR/M001288/1), the Wellcome Trust (105727/Z/14/Z) and British Heart Foundation (PG/14/79/31102 and PG/15/12/31280), and the Isaac Newton Trust/Wellcome Trust ISSF/University of Cambridge Joint Research Grants Scheme (to JAF).

Data availability

Not applicable

References:

- Ahern, G. P., Junankar, P. R. and Dulhunty, A. F. (1994). Single channel activity of the ryanodine receptor calcium release channel is modulated by FK-506. *FEBS Lett.* **352**, 369–374.
- Allouis, M., Probst, V., Jaafar, P., Schott, J. J. and Le Marec, H. (2005). Unusual clinical presentation in a family with catecholaminergic polymorphic ventricular tachycardia due to a G14876A ryanodine receptor gene mutation. *Am. J. Cardiol.* **95**, 700–702.
- Benjamin, E. J., Wolf, P. A., D'Agostino, R. B., Silbershatz, H., Kannel, W. B. and Levy, D. (1998). Impact of atrial fibrillation on the risk of death: the Framingham Heart Study. *Circulation* **98**, 946–952.
- Bers, D. M. (2001). *Excitation-Contraction Coupling and Cardiac Contractile Force*. Springer Netherlands.
- Blayney, L., Beck, K., MacDonald, E., D'Cruz, L., Nomikos, M., Griffiths, J., Thanassoulas, A., Nounesis, G. and Lai, F. A. (2013). ATP interacts with the CPVT mutation-associated central domain of the cardiac ryanodine receptor. *Biochim. Biophys. Acta - Gen. Subj.* **1830**, 4426–4432.
- Brillantes, A. M. B., Ondrias, K., Scott, A., Kobrinsky, E., Ondriašová, E., Moschella, M. C., Jayaraman, T., Landers, M., Ehrlich, B. E. and Marks, A. R. (1994). Stabilization of calcium release channel (ryanodine receptor) function by FK506-binding protein. *Cell* **77**, 513–523.
- Cerrone, M., Colombi, B., Santoro, M., di Barletta, M. R., Scelsi, M., Villani, L., Napolitano, C. and Priori, S. G. (2005). Bidirectional Ventricular Tachycardia and Fibrillation Elicited in a Knock-In Mouse Model Carrier of a Mutation in the Cardiac Ryanodine Receptor. *Circ. Res.* **96**, e77–e82.
- Copello, J. A., Barg, S., Onoue, H. and Fleischer, S. (1997). Heterogeneity of Ca²⁺ gating of skeletal muscle and cardiac ryanodine receptors. *Biophys. J.* **73**, 141–156.
- D'Amati, G., Bagattin, A., Bauce, B., Rampazzo, A., Autore, C., Basso, C., King, K., Romeo, M. D., Gallo, P., Thiene, G., et al. (2005). Juvenile sudden death in a family with polymorphic ventricular arrhythmias caused by a novel RyR2 gene mutation: Evidence of specific morphological substrates. *Hum. Pathol.* **36**, 761–767.
- Davis, R. C., Hobbs, F. D. R., Kenkre, J. E., Roalfe, A. K., Iles, R., Lip, G. Y. H. and Davies, M. K. (2012). Prevalence of atrial fibrillation in the general population and in high-risk groups: the ECHOES study. *Europace* **14**, 1553–1559.
- Denniss, A., Dulhunty, A. F. and Beard, N. A. (2018). Ryanodine receptor Ca²⁺ release channel post-translational modification: Central player in cardiac and skeletal muscle disease. *Int. J. Biochem. Cell Biol.* **101**, 49–53.
- des Georges, A., Clarke, O. B., Zalk, R., Yuan, Q., Condon, K. J., Grassucci, R. A., Hendrickson, W. A., Marks, A. R. and Frank, J. (2016). Structural Basis for Gating and Activation of RyR1. *Cell* **167**, 145–157.e17.
- Dhindwal, S., Lobo, J., Cabra, V., Santiago, D. J., Nayak, A. R., Dryden, K. and Samsó, M. (2017). A cryo-EM-based model of phosphorylation- and FKBP12.6-mediated allosterism of the cardiac ryanodine receptor. *Sci. Signal.* **10**, eaai8842.
- Dobrev, D. and Wehrens, X. H. T. (2014). Role of RyR2 Phosphorylation in Heart Failure and Arrhythmias: Controversies Around Ryanodine Receptor Phosphorylation in Cardiac Disease. *Circ. Res.* **114**, 1311–1319.
- Dulhunty, A. F., Laver, D. R., Gallant, E. M., Casarotto, M. G., Pace, S. M. and Curtis, S. (1999). Activation and Inhibition of Skeletal RyR Channels by a Part of the Skeletal DHPR II-III Loop: Effects of DHPR Ser 687 and FKBP12. *Biophys. J.* **77**, 189–203.
- Feng, W., Liu, G., Allen, P. D. and Pessah, I. N. (2000). Transmembrane Redox Sensor of Ryanodine Receptor Complex. *J. Biol. Chem.* **275**, 35902–35907.

- Friel, D. D. and Tsien, R. W.** (1989). Voltage-gated calcium channels: direct observation of the anomalous mole fraction effect at the single-channel level. *Proc. Natl. Acad. Sci.* **86**, 5207–5211.
- Galfré, E., Pitt, S. J., Venturi, E., Sitsapesan, M., Zaccai, N. R., Tsaneva-Atanasova, K., O'Neill, S. and Sitsapesan, R.** (2012). FKBP12 Activates the Cardiac Ryanodine Receptor Ca²⁺-Release Channel and Is Antagonised by FKBP12.6. *PLoS One* **7**, e31956.
- Gillespie, D., Xu, L., Wang, Y. and Meissner, G.** (2005). (De)constructing the ryanodine receptor: Modeling ion permeation and selectivity of the calcium release channel. *J. Phys. Chem. B* **109**, 15598–15610.
- Glukhov, A. V, Kalyanasundaram, A., Lou, Q., Hage, L. T., Hansen, B. J., Belevych, A. E., Mohler, P. J., Knollmann, B. C., Periasamy, M., Györke, S., et al.** (2015). Calsequestrin 2 deletion causes sinoatrial node dysfunction and atrial arrhythmias associated with altered sarcoplasmic reticulum calcium cycling and degenerative fibrosis within the mouse atrial pacemaker complex1. *Eur. Heart J.* **36**, 686–697.
- Goddard, C. A., Ghais, N. S., Zhang, Y., Williams, A. J., Colledge, W. H., Grace, A. A. and Huang, C. L.-H.** (2008). Physiological consequences of the P2328S mutation in the ryanodine receptor (RyR2) gene in genetically modified murine hearts. *Acta Physiol.* **194**, 123–140.
- Hanna, A. D., Lam, A., Thekkedam, C., Gallant, E. M., Beard, N. A. and Dulhunty, A. F.** (2014). Cardiac ryanodine receptor activation by a high Ca²⁺ store load is reversed in a reducing cytoplasmic redox environment. *J. Cell Sci.* **127**, 4531–41.
- Hewawasam, R., Liu, D., Casarotto, M. G., Dulhunty, A. F. and Board, P. G.** (2010). The structure of the C-terminal helical bundle in glutathione transferase M2-2 determines its ability to inhibit the cardiac ryanodine receptor. *Biochem. Pharmacol.* **80**, 381–388.
- Huang, C. L.-H.** (2017). Murine Electrophysiological Models of Cardiac Arrhythmogenesis. *Physiol. Rev.* **97**, 283–409.
- Jiang, D., Wang, R., Xiao, B., Kong, H., Hunt, D. J., Choi, P., Zhang, L. and Chen, S. R. W.** (2005). Enhanced Store Overload-Induced Ca²⁺ Release and Channel Sensitivity to Luminal Ca²⁺ Activation Are Common Defects of RyR2 Mutations Linked to Ventricular Tachycardia and Sudden Death. *Circ. Res.* **97**, 1173–1181.
- Jiang, D., Chen, W., Wang, R., Zhang, L. and Chen, S. R. W.** (2007). Loss of luminal Ca²⁺ activation in the cardiac ryanodine receptor is associated with ventricular fibrillation and sudden death. *Proc. Natl. Acad. Sci.* **104**, 18309–18314.
- Jones, P. P., Guo, W. and Chen, S. R. W.** (2017). Control of cardiac ryanodine receptor by sarcoplasmic reticulum luminal Ca²⁺. *J. Gen. Physiol.* **149**, 867–875.
- King, J. H., Zhang, Y., Lei, M., Grace, A. A., Huang, C. L.-H. and Fraser, J. A.** (2013). Atrial arrhythmia, triggering events and conduction abnormalities in isolated murine RyR2-P2328S hearts. *Acta Physiol.* **207**, 308–323.
- Kourliouros, A., Savelieva, I., Kiotsekoglou, A., Jahangiri, M. and Camm, J.** (2009). Current concepts in the pathogenesis of atrial fibrillation. *Am. Heart J.* **157**, 243–252.
- Laemmli, U. K.** (1970). Cleavage of structural proteins during the assembly of the head of bacteriophage T4. *Nature* **227**, 680–685.
- Laitinen, P. J., Brown, K. M., Piippo, K., Swan, H., Devaney, J. M., Brahmabhatt, B., Donarum, E. A., Marino, M., Tiso, N., Viitasalo, M., et al.** (2001). Mutations of the Cardiac Ryanodine Receptor (RyR2) Gene in Familial Polymorphic Ventricular Tachycardia. *Circulation* **103**, 485–490.
- Lam, E., Martin, M. M., Timerman, A. P., Sabers, C., Fleischer, S., Lukas, T., Abraham, R. T., O'Keefe, S. J., O'Neill, E. A. and Wiederrecht, G. J.** (1995). A novel FK506 binding protein can mediate the immunosuppressive effects of FK506 and is associated with the cardiac ryanodine receptor. *J. Biol. Chem.* **270**, 26511–26522.

- Laver, D. R.** (2007). Ca^{2+} Stores Regulate Ryanodine Receptor Ca^{2+} Release Channels via Luminal and Cytosolic Ca^{2+} Sites. *Biophys. J.* **92**, 3541–3555.
- Laver, D. R.** (2010). Regulation of RyR channel gating by Ca^{2+} , Mg^{2+} and ATP. *Curr. Top. Membr.* **66**, 69–89.
- Laver, D. R.** (2018). Regulation of the RyR channel gating by Ca^{2+} and Mg^{2+} . *Biophys. Rev.* **10**, 1087–1095.
- Laver, D. R. and Lamb, G. D.** (1998). Inactivation of Ca^{2+} release channels (ryanodine receptors RyR1 and RyR2) with rapid steps in $[\text{Ca}^{2+}]$ and voltage. *Biophys. J.* **74**, 2352–64.
- Laver, D. R., Roden, L. D., Ahern, G. P., Eager, K. R., Junankar, P. R. and Dulhunty, A. F.** (1995). Cytoplasmic Ca^{2+} inhibits the ryanodine receptor from cardiac muscle. *J. Membr. Biol.* **147**, 7–22.
- Laver, D. R., Baynes, T. M. and Dulhunty, A. F.** (1997a). Magnesium inhibition of ryanodine-receptor calcium channels: Evidence for two independent mechanisms. *J. Membr. Biol.* **156**, 213–229.
- Laver, D. R., Owen, V. J., Junankar, P. R., Taske, N. L., Dulhunty, A. F. and Lamb, G. D.** (1997b). Reduced inhibitory effect of Mg^{2+} on ryanodine receptor- Ca^{2+} release channels in malignant hyperthermia. *Biophys. J.* **73**, 1913–1924.
- Lehnart, S. E., Wehrens, X. H. T., Laitinen, P. J., Reiken, S. R., Deng, S.-X., Cheng, Z., Landry, D. W., Kontula, K., Swan, H. and Marks, A. R.** (2004). Sudden Death in Familial Polymorphic Ventricular Tachycardia Associated With Calcium Release Channel (Ryanodine Receptor) Leak. *Circulation* **109**, 3208–3214.
- Lehnart, S. E., Mongillo, M., Bellinger, A., Lindegger, N., Chen, B. X., Hsueh, W., Reiken, S., Wronska, A., Drew, L. J., Ward, C. W., et al.** (2008). Leaky Ca^{2+} release channel/ryanodine receptor 2 causes seizures and sudden cardiac death in mice. *J. Clin. Invest.* **118**, 2230–2245.
- Li, J., Imtiaz, M. S., Beard, N. A., Dulhunty, A. F., Thorne, R., VanHelden, D. F. and Laver, D. R.** (2013). β -Adrenergic stimulation increases RyR2 activity via intracellular Ca^{2+} and Mg^{2+} regulation. *PLoS One* **8**, e58334.
- Liu, N. and Priori, S. G.** (2007). Disruption of calcium homeostasis and arrhythmogenesis induced by mutations in the cardiac ryanodine receptor and calsequestrin. *Cardiovasc. Res.* **77**, 293–301.
- Liu, N., Colombi, B., Memmi, M., Zissimopoulos, S., Rizzi, N., Negri, S., Imbriani, M., Napolitano, C., Lai, F. A. and Priori, S. G.** (2006). Arrhythmogenesis in Catecholaminergic Polymorphic Ventricular Tachycardia: Insights From a RyR2 R4496C Knock-In Mouse Model. *Circ. Res.* **99**, 292–298.
- Liu, Y., Kimlicka, L., Hiess, F., Tian, X., Wang, R., Zhang, L., Jones, P. P., Van Petegem, F. and Chen, S. R. W.** (2013). The CPVT-associated RyR2 mutation G230C enhances store overload-induced Ca^{2+} release and destabilizes the N-terminal domains. *Biochem. J.* **454**, 123–131.
- Marks, A. R.** (2002). Ryanodine receptors, FKBP12, and heart failure. *Front. Biosci.* **7**, d970-7.
- Marx, S. O. and Marks, A. R.** (2002). Regulation of the ryanodine receptor in heart failure. *Basic Res. Cardiol.* **97 Suppl 1**, I49-51.
- Marx, S. O., Reiken, S., Hisamatsu, Y., Jayaraman, T., Burkhoff, D., Rosemblyt, N. and Marks, A. R.** (2000). PKA phosphorylation dissociates FKBP12.6 from the calcium release channel (ryanodine receptor): Defective regulation in failing hearts. *Cell* **101**, 365–376.
- Meli, A. C., Refaat, M. M., Dura, M., Reiken, S., Wronska, A., Wojciak, J., Carroll, J., Scheinman, M. M. and Marks, A. R.** (2011). A novel ryanodine receptor mutation linked to sudden death increases sensitivity to cytosolic calcium. *Circ. Res.* **109**, 281–90.

- Ning, F., Luo, L., Ahmad, S., Valli, H., Jeevaratnam, K., Wang, T., Guzadhur, L., Yang, D., Fraser, J. A., Huang, C. L. H., et al.** (2016). The RyR2-P2328S mutation downregulates Nav1.5 producing arrhythmic substrate in murine ventricles. *Pflugers Arch. Eur. J. Physiol.* **468**, 655–665.
- Oda, T., Yang, Y., Uchinoumi, H., Thomas, D. D., Chen-Izu, Y., Kato, T., Yamamoto, T., Yano, M., Cornea, R. L. and Bers, D. M.** (2015). Oxidation of ryanodine receptor (RyR) and calmodulin enhance Ca release and pathologically alter, RyR structure and calmodulin affinity. *J. Mol. Cell. Cardiol.* **85**, 240–248.
- Paavola, J., Viitasalo, M., Laitinen-Forsblom, P. J., Pasternack, M., Swan, H., Tikkanen, I., Toivonen, L., Kontula, K. and Laine, M.** (2007). Mutant ryanodine receptors in catecholaminergic polymorphic ventricular tachycardia generate delayed afterdepolarizations due to increased propensity to Ca²⁺ waves. *Eur. Heart J.* **28**, 1135–1142.
- Paech, C., Gebauer, R. A., Karstedt, J., Marschall, C., Bollmann, A. and Husser, D.** (2014). Ryanodine Receptor Mutations Presenting as Idiopathic Ventricular Fibrillation: A Report on Two Novel Familial Compound Mutations, c.6224T>C and c.13781A>G, with the Clinical Presentation of Idiopathic Ventricular Fibrillation. *Pediatr. Cardiol.* **35**, 1437–1441.
- Pessah, I. N., Kim, K. H. and Feng, W.** (2002). Redox sensing properties of the ryanodine receptor complex. *Front. Biosci.* **7**, a72-9.
- Pizzale, S., Gollob, M. H., Gow, R. and Birnie, D. H.** (2008). Sudden death in a young man with catecholaminergic polymorphic ventricular tachycardia and paroxysmal atrial fibrillation. *J. Cardiovasc. Electrophysiol.* **19**, 1319–1321.
- Postma, A. V., Denjoy, I., Kamblock, J., Alders, M., Lupoglazoff, J. M., Vaksman, G., Dubosq-Bidot, L., Sebillon, P., Mannens, M. M. A. M., Guicheney, P., et al.** (2005). Catecholaminergic polymorphic ventricular tachycardia: RYR2 mutations, bradycardia, and follow up of the patients. *J. Med. Genet.* **42**, 863–870.
- Priori, S. G. and Chen, S. R. W.** (2011). Inherited dysfunction of sarcoplasmic reticulum Ca²⁺ handling and arrhythmogenesis. *Circ. Res.* **108**, 871–883.
- Priori, S. G., Napolitano, C., Tiso, N., Memmi, M., Vignati, G., Bloise, R., Sorrentino, V. and Danieli, G. A.** (2001). Mutations in the cardiac ryanodine receptor gene (hRyR2) underlie catecholaminergic polymorphic ventricular tachycardia. *Circulation* **103**, 196–200.
- Richardson, S. J., Steele, G. A., Gallant, E. M., Lam, A., Schwartz, C. E., Board, P. G., Casarotto, M. G., Beard, N. A. and Dulhunty, A. F.** (2017). Association of FK506 binding proteins with RyR channels – effect of CLIC2 binding on sub-conductance opening and FKBP binding. *J. Cell Sci.* **130**, 3588–3600.
- Ronen, B. J. and Lili, B.** (2016). Patient specific induced pluripotent stem cell-derived cardiomyocytes for drug development and screening in catecholaminergic polymorphic ventricular Tachycardia. *J. Atr. Fibrillation* **9**, 91–97.
- Sabir, I. N., Ma, N., Jones, V. J., Goddard, C. a, Zhang, Y., Kalin, A., Grace, A. a and Huang, C. L. H.** (2010). Alternans in genetically modified langendorff-perfused murine hearts modeling catecholaminergic polymorphic ventricular tachycardia. *Front. Physiol.* **1**, 126.
- Salvage, S. C., King, J. H., Chandrasekharan, K. H., Jafferji, D. I. G., Guzadhur, L., Matthews, H. R., Huang, C. L. H. and Fraser, J. A.** (2015). Flecainide exerts paradoxical effects on sodium currents and atrial arrhythmia in murine RyR2-P2328S hearts. *Acta Physiol.* **214**, 361–375.
- Schlotthauer, K. and Bers, D. M.** (2000). Sarcoplasmic reticulum Ca²⁺ release causes myocyte depolarization: Underlying mechanism and threshold for triggered action potentials. *Circ. Res.* **87**, 774–780.

- Shan, J., Betzenhauser, M. J., Kushnir, A., Reiken, S., Meli, A. C., Wronska, A., Dura, M., Chen, B. X. and Marks, A. R.** (2010). Role of chronic ryanodine receptor phosphorylation in heart failure and β -adrenergic receptor blockade in mice. *J. Clin. Invest.* **120**, 4375–4387.
- Shan, J., Xie, W., Betzenhauser, M., Reiken, S., Chen, B.-X., Wronska, A. and Marks, A. R.** (2012). Calcium Leak Through Ryanodine Receptors Leads to Atrial Fibrillation in 3 Mouse Models of Catecholaminergic Polymorphic Ventricular Tachycardia. *Circ. Res.* **111**, 708–717.
- Sigalas, C., Mayo-Martin, M. B., Jane, D. E. and Sitsapesan, R.** (2009). Ca^{2+} -Calmodulin Increases RyR2 Open Probability yet Reduces Ryanoid Association with RyR2. *Biophys. J.* **97**, 1907–1916.
- Sitsapesan, R. and Williams, A. J.** (1994). Regulation of the gating of the sheep cardiac sarcoplasmic reticulum Ca^{2+} -release channel by luminal Ca^{2+} . *J. Membr. Biol.* **137**, 215–226.
- Sumitomo, N.** (2016). Current topics in catecholaminergic polymorphic ventricular tachycardia. *J. Arrhythmia* **32**, 344–351.
- Sumitomo, N., Sakurada, H., Taniguchi, K., Matsumura, M., Abe, O., Miyashita, M., Kanamaru, H., Karasawa, K., Ayusawa, M., Fukamizu, S., et al.** (2007). Association of Atrial Arrhythmia and Sinus Node Dysfunction in Patients With Catecholaminergic Polymorphic Ventricular Tachycardia. *Circ. J.* **71**, 1606–1609.
- Swan, H., Piippo, K., Viitasalo, M., Heikkilä, P., Paavonen, T., Kainulainen, K., Kere, J., Keto, P., Kontula, K. and Toivonen, L.** (1999). Arrhythmic disorder mapped to chromosome 1q42–q43 causes malignant polymorphic ventricular tachycardia in structurally normal hearts. *J. Am. Coll. Cardiol.* **34**, 2035–2042.
- Timerman, A. P., Onoue, H., Xin, H. B., Barg, S., Copello, J., Wiederrecht, G. and Fleischer, S.** (1996). Selective binding of FKBP12.6 by the cardiac ryanodine receptor. *J. Biol. Chem.* **271**, 20385–20391.
- Tiso, N., Salamon, M., Bagattin, A., Danieli, G. A., Argenton, F. and Bortolussi, M.** (2002). The binding of the RyR2 calcium channel to its gating protein FKBP12.6 is oppositely affected by ARVD2 and VTSIP mutations. *Biochem. Biophys. Res. Commun.* **299**, 594–598.
- Towbin, H., Staehelin, T. and Gordon, J.** (1979). Electrophoretic transfer of proteins from polyacrylamide gels to nitrocellulose sheets: procedure and some applications. *Proc. Natl. Acad. Sci.* **76**, 4350–4354.
- Tripathy, A. and Meissner, G.** (1996). Sarcoplasmic reticulum lumenal Ca^{2+} has access to cytosolic activation and inactivation sites of skeletal muscle Ca^{2+} release channel. *Biophys. J.* **70**, 2600–2615.
- Vest, J. A., Wehrens, X. H. T., Reiken, S. R., Lehnart, S. E., Dobrev, D., Chandra, P., Danilo, P., Ravens, U., Rosen, M. R. and Marks, A. R.** (2005). Defective cardiac ryanodine receptor regulation during atrial fibrillation. *Circulation* **111**, 2025–2032.
- Walweel, K., Li, J., Molenaar, P., Imtiaz, M. S., Quail, A., dos Remedios, C. G., Beard, N. A., Dulhunty, A. F., van Helden, D. F. and Laver, D. R.** (2014). Differences in the regulation of RyR2 from human, sheep, and rat by Ca^{2+} and Mg^{2+} in the cytoplasm and in the lumen of the sarcoplasmic reticulum. *J. Gen. Physiol.* **144**, 263–271.
- Walweel, K., Molenaar, P., Imtiaz, M. S., Denniss, A., dos Remedios, C., van Helden, D. F., Dulhunty, A. F., Laver, D. R. and Beard, N. A.** (2017). Ryanodine receptor modification and regulation by intracellular Ca^{2+} and Mg^{2+} in healthy and failing human hearts. *J. Mol. Cell. Cardiol.* **104**, 53–62.
- Wehrens, X. H. T., Lehnart, S. E., Huang, F., Vest, J. A., Reiken, S. R., Mohler, P. J., Sun, J., Guatimosim, S., Song, L.-S., Rosemblyt, N., et al.** (2003). FKBP12.6 Deficiency and Defective Calcium Release Channel (Ryanodine Receptor) Function Linked to Exercise-Induced Sudden Cardiac Death. *Cell* **113**, 829–840.

- Xiao, J., Tian, X., Jones, P. P., Bolstad, J., Kong, H., Wang, R., Zhang, L., Duff, H. J., Gillis, A. M., Fleischer, S., et al.** (2007). Removal of FKBP12.6 Does Not Alter the Conductance and Activation of the Cardiac Ryanodine Receptor or the Susceptibility to Stress-induced Ventricular Arrhythmias. *J. Biol. Chem.* **282**, 34828–34838.
- Xiao, Z., Guo, W., Sun, B., Hunt, D. J., Wei, J., Liu, Y., Wang, Y., Wang, R., Jones, P. P., Back, T. G., et al.** (2016). Enhanced cytosolic Ca^{2+} activation underlies a common defect of central domain cardiac ryanodine receptor mutations linked to arrhythmias. *J. Biol. Chem.* **291**, 24528–24537.
- Xu, L. and Meissner, G.** (1998). Regulation of cardiac muscle Ca^{2+} release channel by sarcoplasmic reticulum luminal Ca^{2+} . *Biophys. J.* **75**, 2302–2312.
- Xu, L., Mann, G. and Meissner, G.** (1996). Regulation of cardiac Ca^{2+} release channel (ryanodine receptor) by Ca^{2+} , H^+ , Mg^{2+} , and adenine nucleotides under normal and simulated ischemic conditions. *Circ. Res.* **79**, 1100–1109.
- Yan, Z., Bai, X., Yan, C., Wu, J., Li, Z., Xie, T., Peng, W., Yin, C., Li, X., Scheres, S. H. W., et al.** (2015). Structure of the rabbit ryanodine receptor RyR1 at near-atomic resolution. *Nature* **517**, 50–55.
- Yano, M., Yamamoto, T., Ikemoto, N. and Matsuzaki, M.** (2005). Abnormal ryanodine receptor function in heart failure. *Pharmacol. Ther.* **107**, 377–391.
- Zhang, Y., Fraser, J. A., Jeevaratnam, K., Hao, X., Hothi, S. S., Grace, A. A., Lei, M. and Huang, C. L.-H.** (2011). Acute atrial arrhythmogenicity and altered Ca^{2+} homeostasis in murine RyR2-P2328S hearts. *Cardiovasc. Res.* **89**, 794–804.
- Zhang, Y., Wu, J., Jeevaratnam, K., King, J. H., Guzadhur, L., Ren, X., Grace, A. A., Lei, M., Huang, C. L.-H. and Fraser, J. A.** (2013). Conduction Slowing Contributes to Spontaneous Ventricular Arrhythmias in Intrinsically Active Murine RyR2-P2328S Hearts. *J. Cardiovasc. Electrophysiol.* **24**, 210–218.
- Zissimopoulos, S. and Lai, F. A.** (2005). Central Domain of the Human Cardiac Muscle Ryanodine Receptor Does Not Mediate Interaction With FKBP12.6. *Cell Biochem. Biophys.* **43**, 203–220.
- Zissimopoulos, S., Seifan, S., Maxwell, C., Williams, A. J. and Lai, F. A.** (2012). Disparities in the association of the ryanodine receptor and the FK506-binding proteins in mammalian heart. *J. Cell Sci.* **125**, 1759–1769.

Table 1. Parameter values for K_A , K_I , Ha and Hi at -40 mV and +40 mV used to fit Hill equations for Ca^{2+} -activation and Ca^{2+} -inhibition of WT and P2328S RyR2 (Figure 4) and for baseline P_o before Ca^{2+} activation (BP_A) and baseline P_o following Ca^{2+} inactivation (BP_I).

	-40 mV						+40 mV					
	K_A	Ha	BP_A	K_I	Hi	BP_I	K_A	Ha	BP_A	K_I	Hi	BP_I
WT	3.5 μM	1.2	0.02	50 mM	1.2	0.05	1.5 μM	1.1	0.014	15 mM	1.2	0.055
P2328S	0.32 μM	1.6	0.1	7 μM	1.0	0.26	0.15 μM	1.8	0.05	1.0 μM	1.3	0.11

Figures

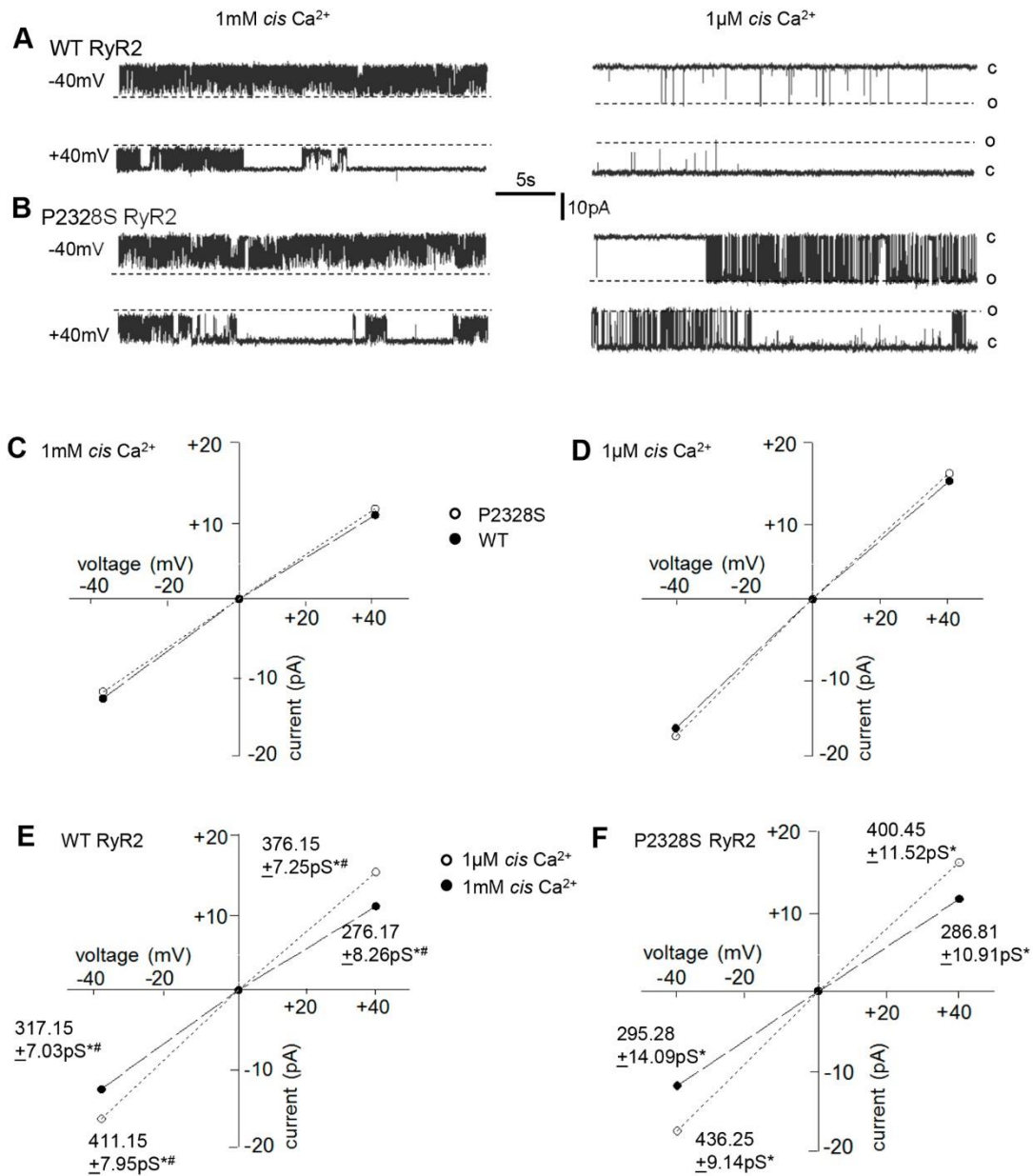


Figure 1. The P2328S mutation enhances RyR2 channel activity when cytoplasmic [Ca²⁺] is 1 μM, without altering maximum channel conductance. (A) and (B) Representative 25 s recordings from one WT RyR2 channel (A) and one P2328S RyR2 channel (B), with 1 mM Ca²⁺ (left panels) or 1 μM cytoplasmic Ca²⁺ (right panels), at -40 mV (upper record) or +40 mV (lower record). Broken lines (o) indicate maximum open currents, and solid lines (c) indicate the closed current levels. (C) and (D) Average maximum single channel currents plotted against voltage with 1 mM (C) or 1 μM (D) Ca²⁺. Long dashed lines through filled circles connect WT data and dotted lines through open circles connect P2328S data. (E) and (F) Data from (C and D) replotted to emphasize the conductance difference between 1 mM with 1 μM Ca²⁺ in WT (B) or P2328S (C) RyR2. Dashed lines through filled circles connect 1 mM Ca²⁺ data and dotted lines through open circles connect 1 μM Ca²⁺ data. Data points include mean ± s.e.m. Error bars are within the symbol dimensions in all

cases. Average conductances \pm SEM values are given beside their respective symbols. N = 20 channels, WT, 1 mM Ca^{2+} , -40 mV; n = 24 channels, WT, 1 μM , -40 mV; n = 22 channels, WT 1 mM Ca^{2+} , +40 mV; n = 23 channels, WT, 1 μM Ca^{2+} , +40 mV. N = 17 channels P2328S, 1 mM Ca^{2+} , -40 mV; n = 21 channels, P2328S, 1 μM Ca^{2+} , -40 mV; n = 18 channels, P2328S 1 mM Ca^{2+} , +40 mV; n = 22 channels, P2328S, 1 μM , +40 mV. # - significant differences between average data at -40 and +40 mV; * - significant difference between conductances with 1 mM and 1 μM Ca^{2+} . There was no significant difference between average WT and P2328S RyR2 conductances under any condition.

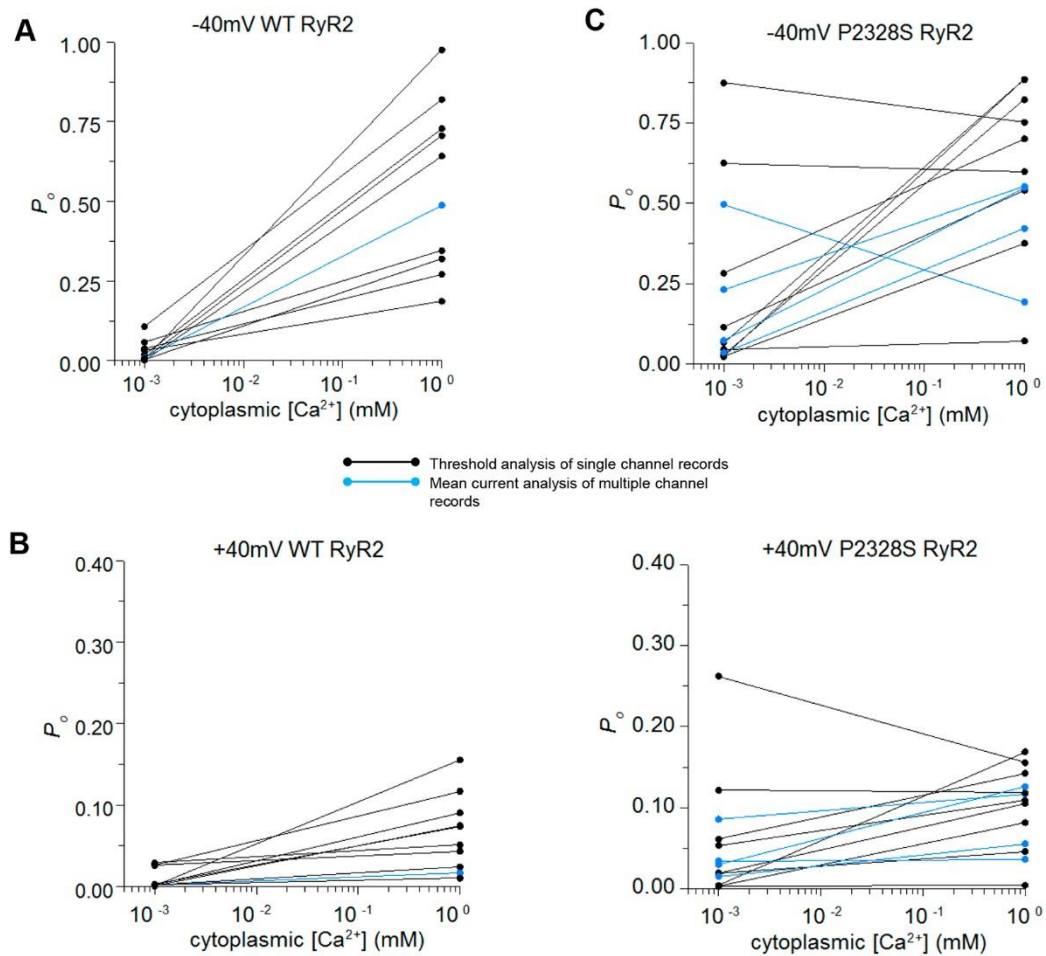


Figure 2. The P_o of individual channels at 1 μM and 1 mM cytoplasmic $[\text{Ca}^{2+}]$ show substantial variability between P2328S channels with 1 μM Ca^{2+} . (A) and (B) WT channels. (C) and (D) P2328S channels. P_o at -40 mV plotted in (A) and (C); P_o at +40 mV plotted in (B) and (D). Black lines link individual channel data from bilayers containing one active channel (P_o determined with a threshold discriminator). Blue lines link measurements from bilayers with more than one channel opening (P_o estimated from I²F: mean current normalized to maximum current - Methods). Notably, P_o values derived from I²F fall within the range of values obtained from direct measurement of P_o .

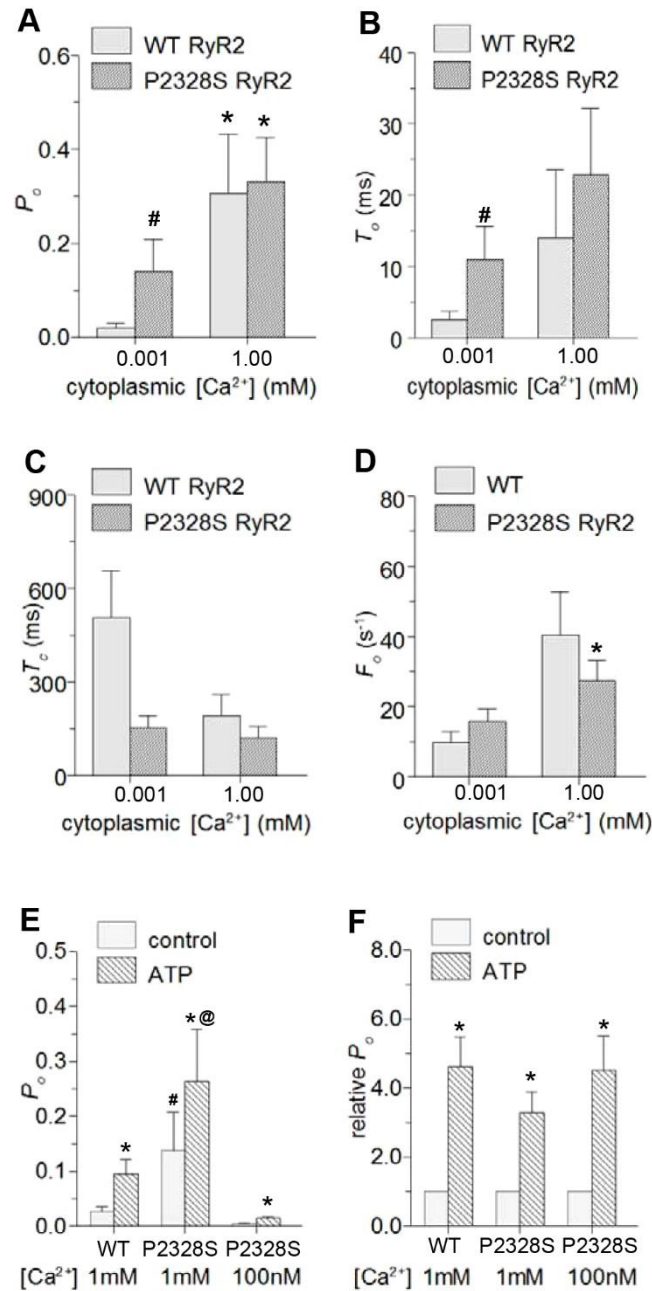


Figure 3. Average gating parameters for WT and P2328S RyR2 channels exposed to 1 μ M or 1mM cytoplasmic Ca^{2+} and effects of ATP reveal significantly higher activity in P2328S with 1 μ M Ca^{2+} . Average data (-40 and +40 mV pooled) for WT (light grey) and P2328S RyR2 (dark grey). (A) – (D) show average values for P_o (WT n = 20; P2328S n=26), T_o (WT n = 16; P2328S n=18), T_c (WT n = 18; P2328S n=20) and F_o (WT n = 18; P2328S n=20). Data is presented as mean \pm s.e.m. * - significant difference between 1 μ M and 1 mM Ca^{2+} . # - significant difference between WT and P2328S. (E) and (F) Average data for WT (n = 7) and P2328S (n = 5) channels before (solid grey bars) and after (cross-hatched bars) exposure to 2 mM ATP, with cytoplasmic Ca^{2+} of 1 μ M (n = 7 WT; n = 5 P2328S) or 100 nM (n = 2 P2328S) as indicated. Absolute P_o (E), relative P_o (F). * - ATP significantly greater than control, # - P2328S control with 1 μ M Ca^{2+}

significantly greater than WT or P2328S control at 100 nM Ca²⁺; @ - P2328S with 1 μM Ca²⁺ plus ATP significantly greater WT with 1 μM Ca²⁺ plus ATP or P2328S with 100 nM Ca²⁺ plus ATP.

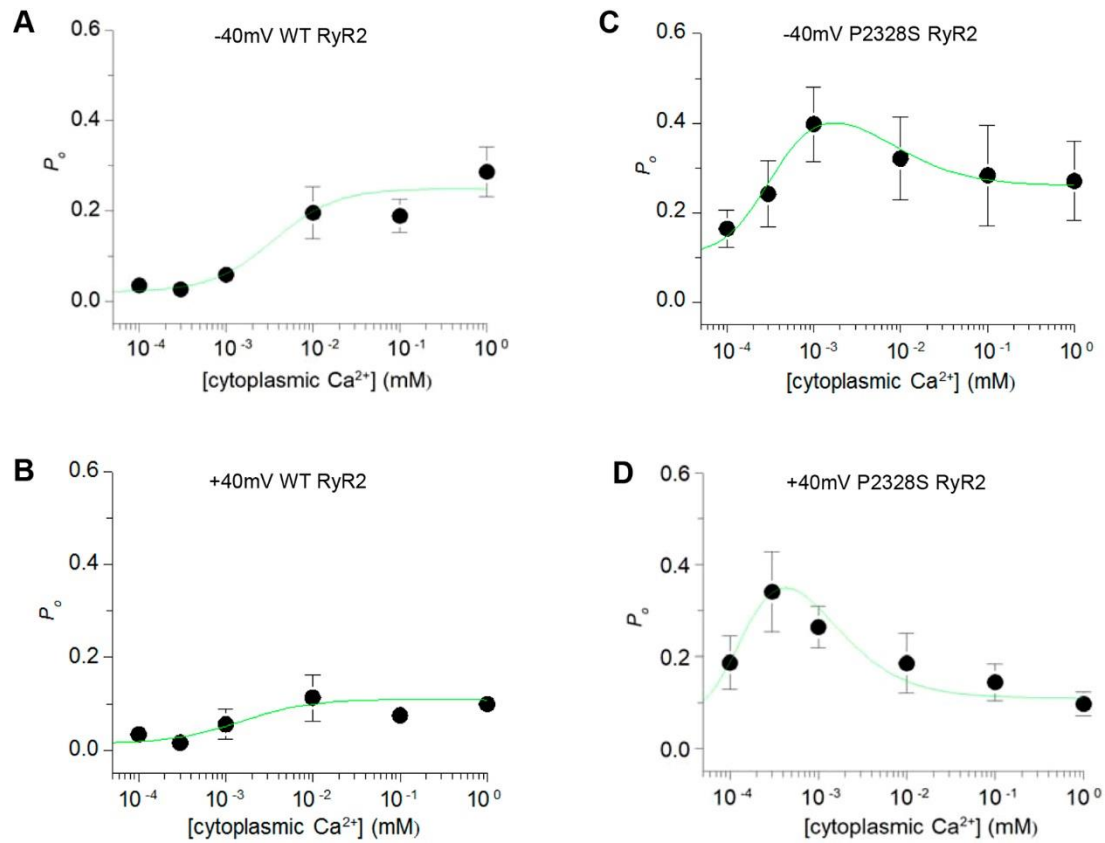


Figure 4. The Ca^{2+} -concentration dependence of P_o reveals substantial effects of the P2328S mutation on Ca^{2+} -activation and Ca^{2+} -inactivation. (A) and (B) Average P_o from experiment #2 for WT RyR2 at -40 and +40 mV respectively. (C) and (D) Average P_o for P2328S RyR2 at -40 and +40 mV respectively. Data points show mean \pm s.e.m. SEM markers are not visible when contained within the dimensions of the symbols. The numbers of observations were the same at -40 and +40 mV for each $[Ca^{2+}]$, but varied between each $[Ca^{2+}]$, depending on whether Ca^{2+} was initially reduced to 100 nM or 300 nM before subsequent concentration increases. For WT channels, $n = x$ ($[Ca^{2+}]$): 4 (100 nM); 3 (300 nM); 12 (1 μ M); 8 (10 μ M); 12 (100 μ M); 8 (1 mM). For P2328S RyR2 channels, $n = ([Ca^{2+}]$): 10 (100 nM); 11 (300 nM); 10 (1 μ M); 7 (10 μ M); 12 (100 μ M); 8 (1 mM). The green line Hill curves fitted to the data using parameters in Table 1.

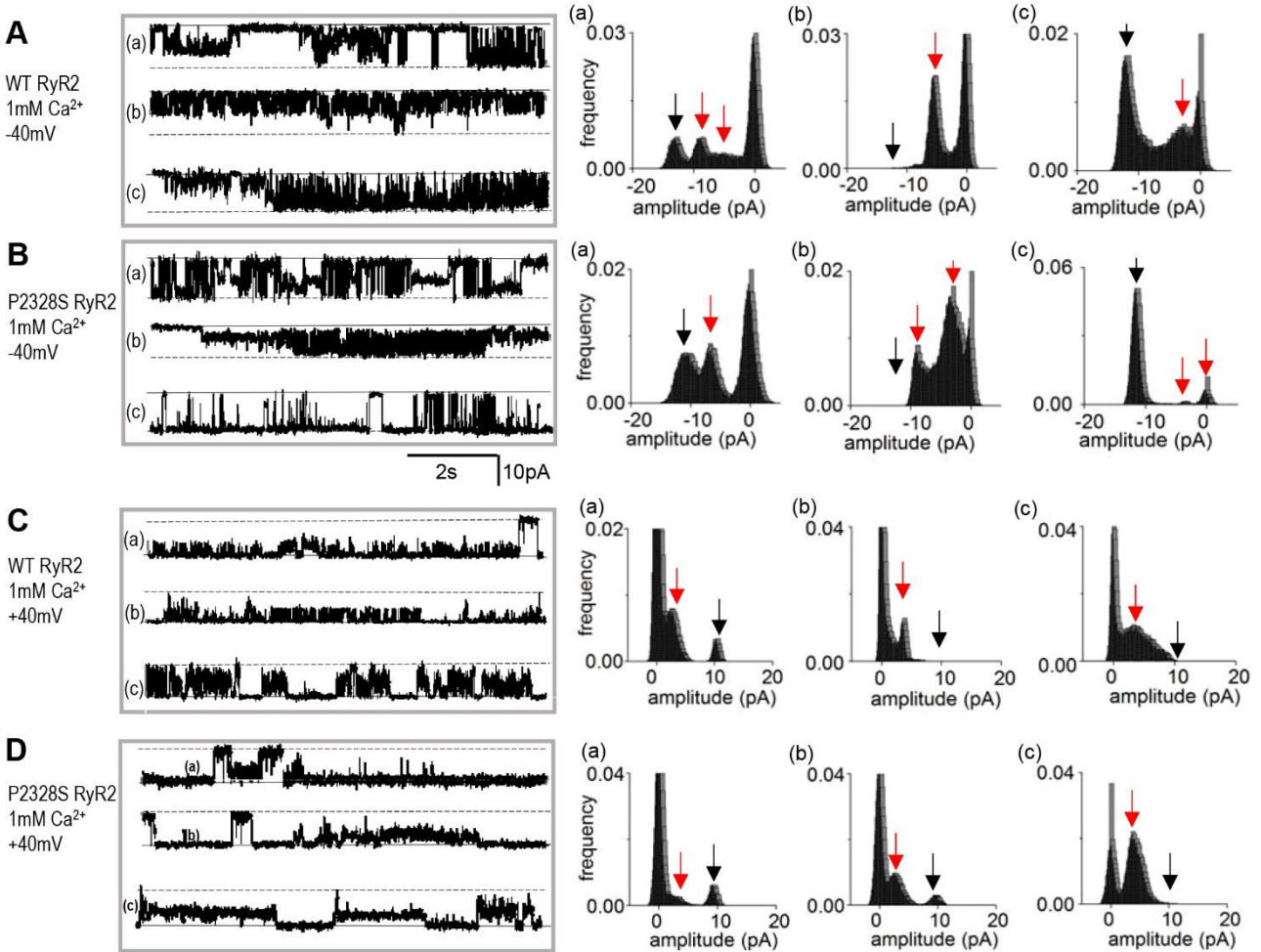


Figure 5. Subconductance openings apparent in both WT and P2328S RyR2 channels with 1 mM cytoplasmic Ca^{2+} . Representative 8.5 s current recordings from 3 different bilayers (a, b and c) shown on the left, with corresponding amplitude histograms on the right. WT at -40 mV (A); P2328S at -40 mV (B); WT at +40 mV (C); P2328S at +40 mV (D). In current records, solid lines indicate the zero current and broken lines indicate maximum open current. In histograms, black arrow points to the maximum single channel current and the red arrows indicate prominent subconductance levels.

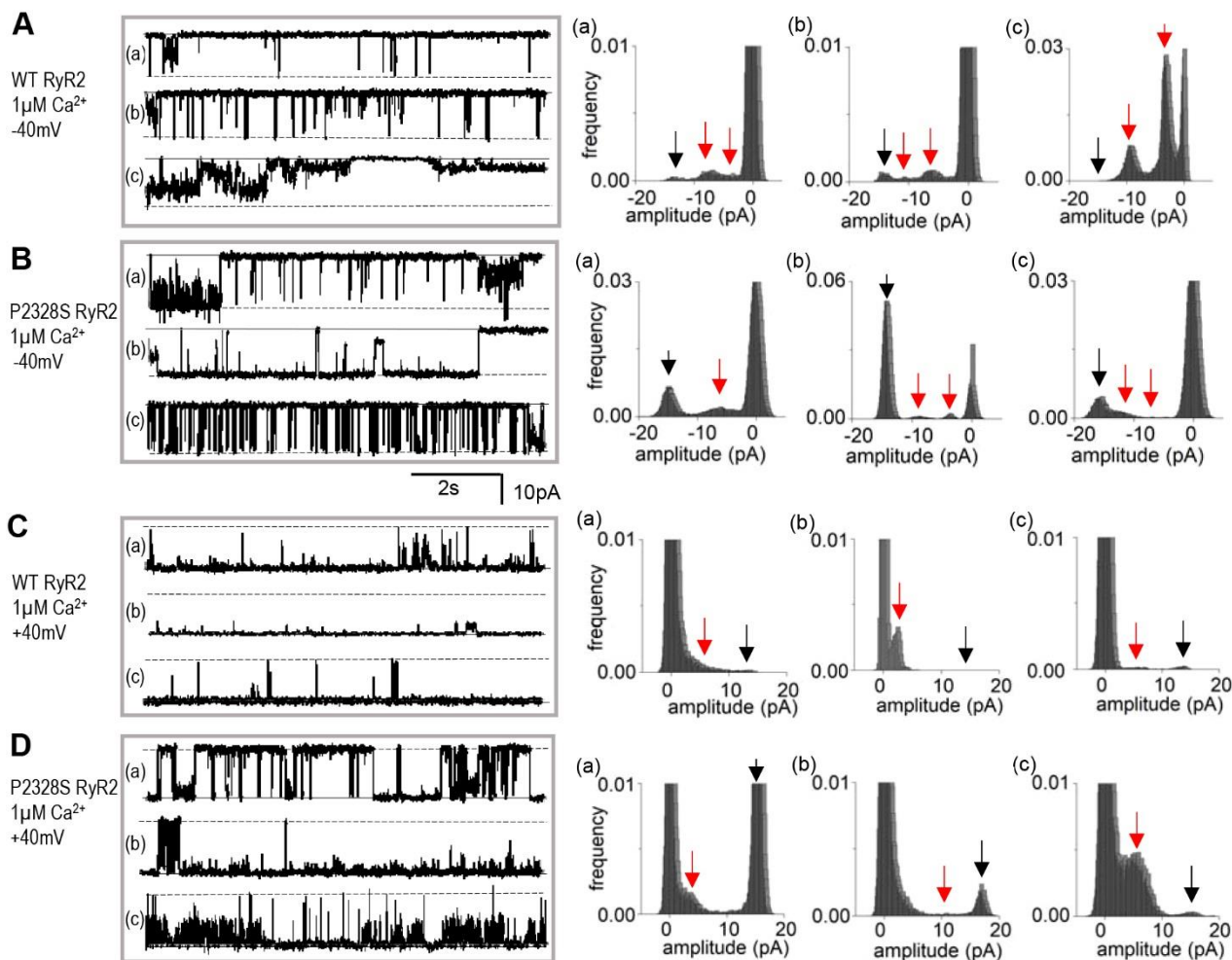


Figure 6. Subconductance openings apparent in WT and P2328S RyR2 channel activity with 1 μ M cytoplasmic Ca²⁺. Representative 8.5 s current recordings from 3 different bilayers (a, b and c) shown on the left, with corresponding amplitude histograms on the right. WT at -40 mV (A); P2328S at -40 mV (B); WT at +40 mV (C); P2328S at +40 mV (D). In current records, solid lines indicate the zero current and the broken lines indicate maximum open current. In histograms, black arrow points to the maximum single channel current and the red arrows indicate prominent subconductance levels.

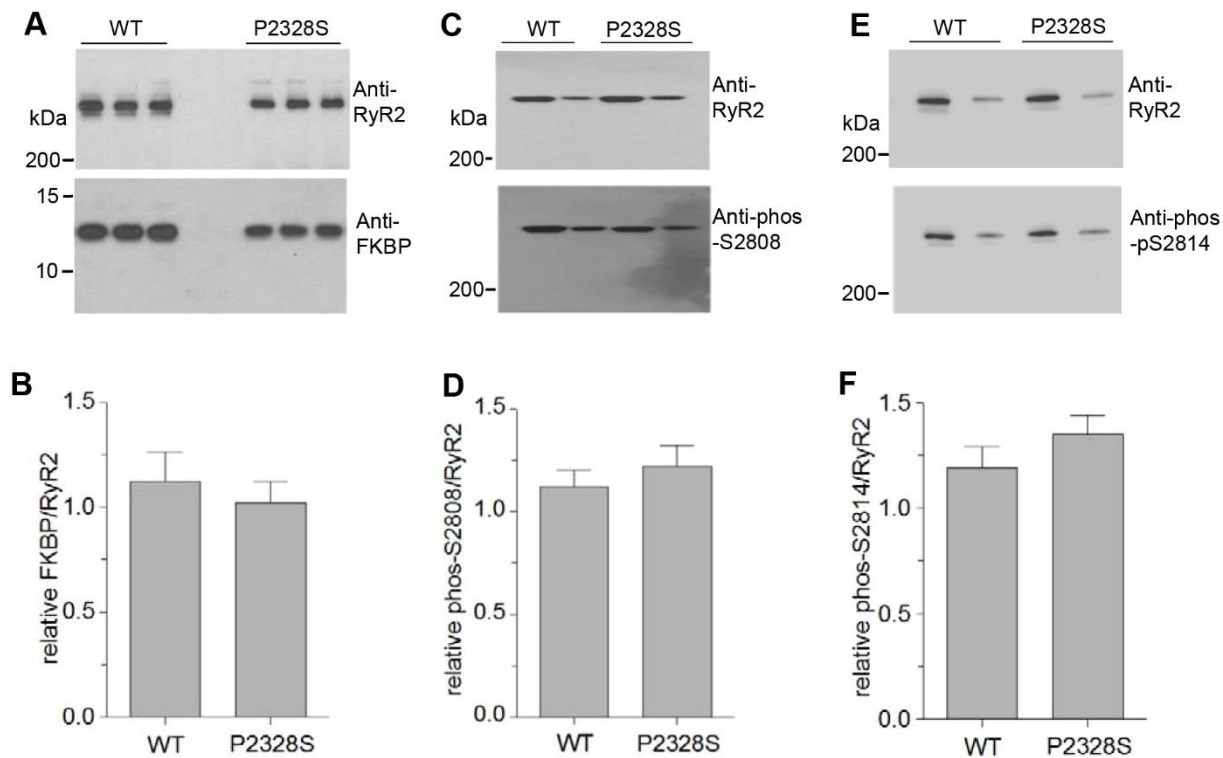


Figure 7. Neither FKBP associated with RyR2 channels nor S2804 or S2814 phosphorylation are altered by the P2328S mutation. (A) Representative blots of RyR2 and associated FKBP12 from WT and RyR2^{S/S} mouse hearts following co-IP of the FKBP/RyR2 complex with anti-RyR2 antibody, SDS-Page and immunoblotting (Methods). (B) Average relative levels of FKBP12 bound to RyR2. FKBP12 band densities normalized to RyR2 band density for each lane, then expressed relative to WT ratios in lane 1. N = 21 for WT and n = 18 for P2328S data. (C) - (F) SR proteins separated via SDS PAGE, subjected to Western Blot and probed with antibodies to phosphorylated (phosphor) S2808 (C) or S2814 (E), then stripped and re-probed with anti-RyR2 as a loading control. Average data for RyR2 phosphorylation at S2808 (D) or S2814 (E). Band densities were normalized to total RyR2, then expressed relative to the WT phos-S2808/RyR2 or phos-S2814/RyR in lane 1. N = 9 for S2808, n = 6 for S2814. Data bars show mean±s.e.m

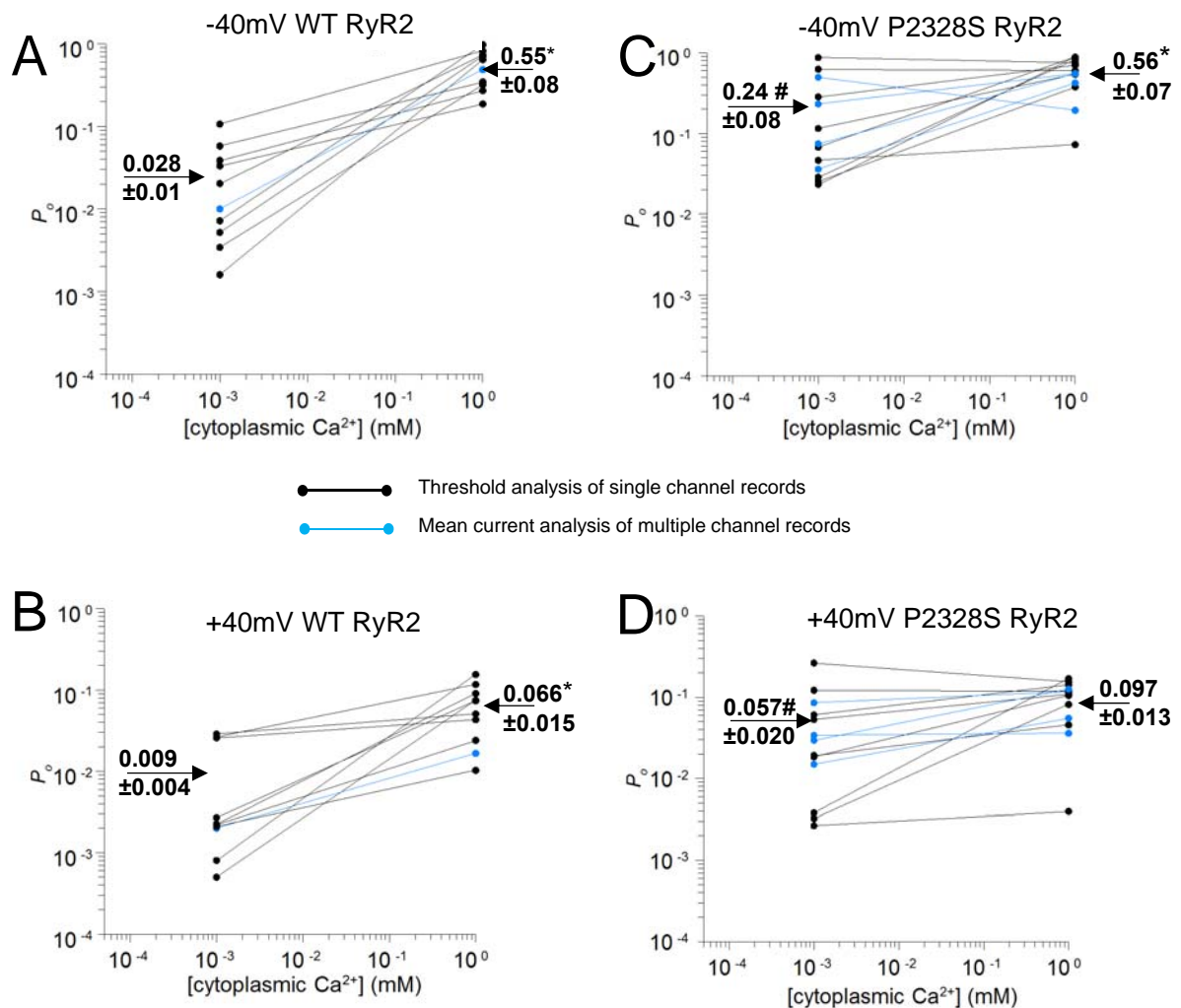


Figure S1. P_o of individual channels at $1 \mu\text{M}$ and 1mM cytoplasmic $[\text{Ca}^{2+}]$ plotted on a logarithmic scale to reveal the spread of data at $1 \mu\text{M}$ cytoplasmic $[\text{Ca}^{2+}]$. (A) and (B) show data for WT channels. (C) and (D) show data for P2328S RyR2 channels. P_o values for recordings at -40mV are shown in (A) and (C), while P_o values for recordings at $+40 \text{mV}$ are shown in (B) and (D). The black lines link P_o measurements from bilayers having one active channel, where P_o was determined using the threshold discriminator method. The blue lines link measurements obtained from bilayers with more than one channel opening at the same time, where P_o is derived from I'_F (mean current normalized to maximum current, as described in the Methods). In (A) – (D), average values for P_o at $1 \mu\text{M}$ cytoplasmic Ca^{2+} are shown to the left of the data points and average values for P_o at 1mM cytoplasmic Ca^{2+} are shown to the right of the data points. The asterisk (*) indicates a significant difference between average P_o at $1 \mu\text{M}$ Ca^{2+} and at 1mM Ca^{2+} . The # symbol indicates a significant difference between average P_o of WT and P2328S RyR2 channels.

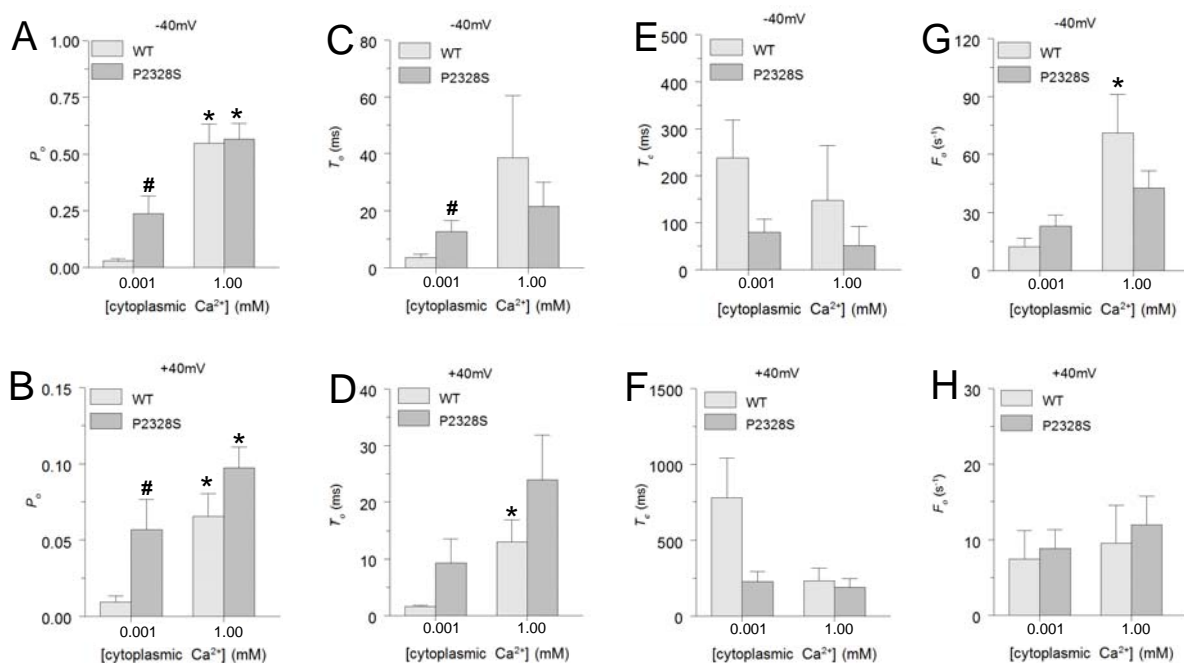


Figure S2. Average gating parameters of WT and P2328S RyR2 channels exposed to 1 μM and 1 mM cytoplasmic Ca²⁺ at -40 mV and at +40 mV. Average data is compared for WT (light grey bars) and P2328S RyR2 (dark grey bars).

(A), (C), (E) and (G) show average values at -40 mV for P_o (WT n = 10; P2328S n=13), T_o (WT n = 8; P2328S n=9), T_c (WT n = 9; P2328S n=10) and F_o (WT n = 9; P2328S n=10), respectively. (B), (D), (F) and (H) show average values, at +40 for P_o (WT n = 10; P2328S n=13), T_o (WT n = 9; P2328S n=10), T_c (WT n = 9; P2328S n=10) and F_o (WT n = 9; P2328S n=10), respectively. Data is presented as mean ± SEM. The asterisk (*) indicates a significant difference between average data at 1 μM Ca²⁺ and at 1 mM Ca²⁺. The # symbol indicates a significant difference between average data for WT and P2328S channels

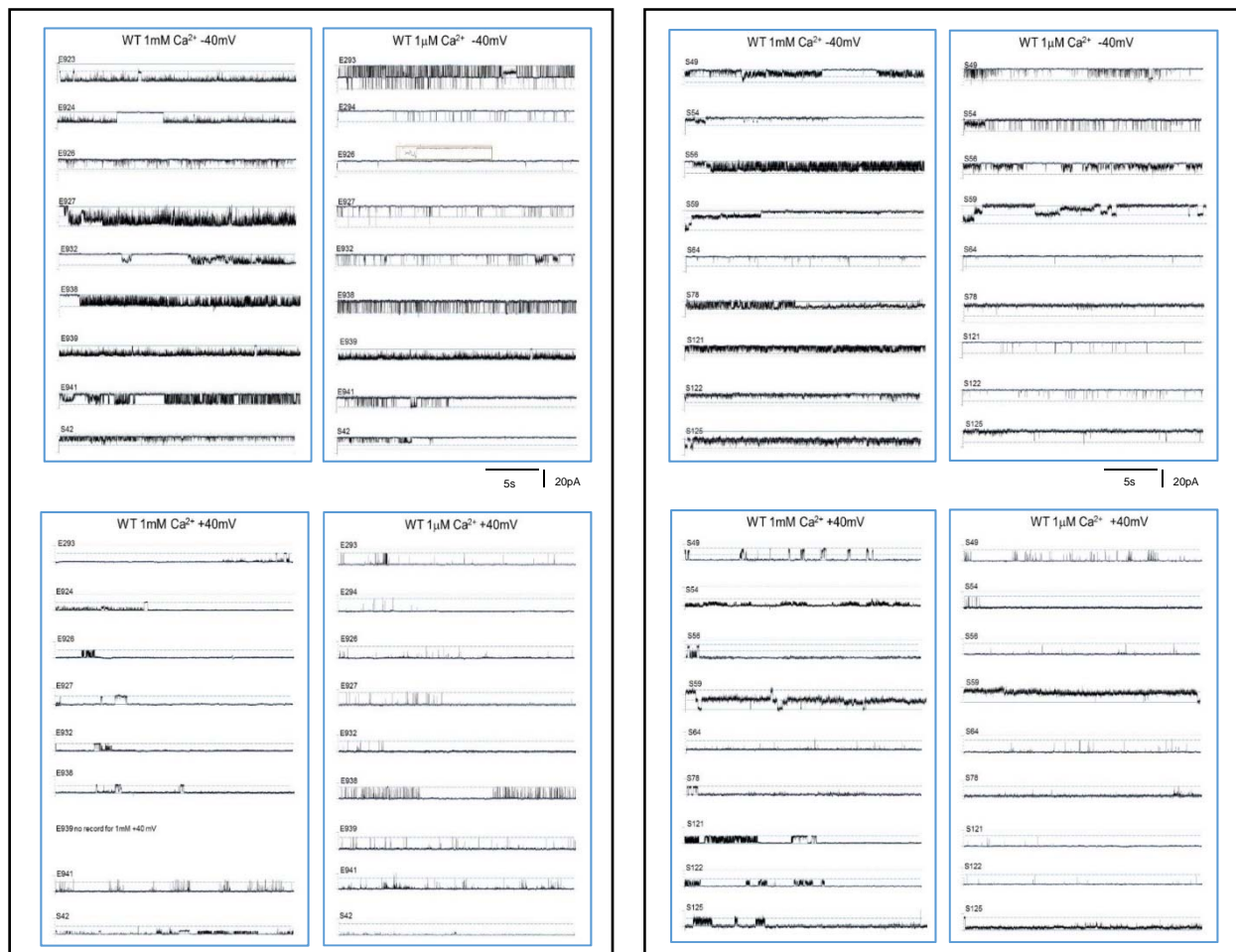


Figure S3. Examples of currents recorded from 18 WT channels used for analyses of channel activity with 1 mM and 1 μ M cytoplasmic Ca^{2+} presented in manuscript Figures 1 to 6. In each panel, records from the same channel are aligned horizontally to allow direct comparisons of the channel activity under each condition. Currents shown on the left hand side of each panel were recorded with 1 mM cytoplasmic Ca^{2+} , while those on the right hand side were recorded with 1 μ M cytoplasmic Ca^{2+} . Currents shown on the top half of each panel were recorded at -40 mV, while those in the lower half were recorded at +40 mV.

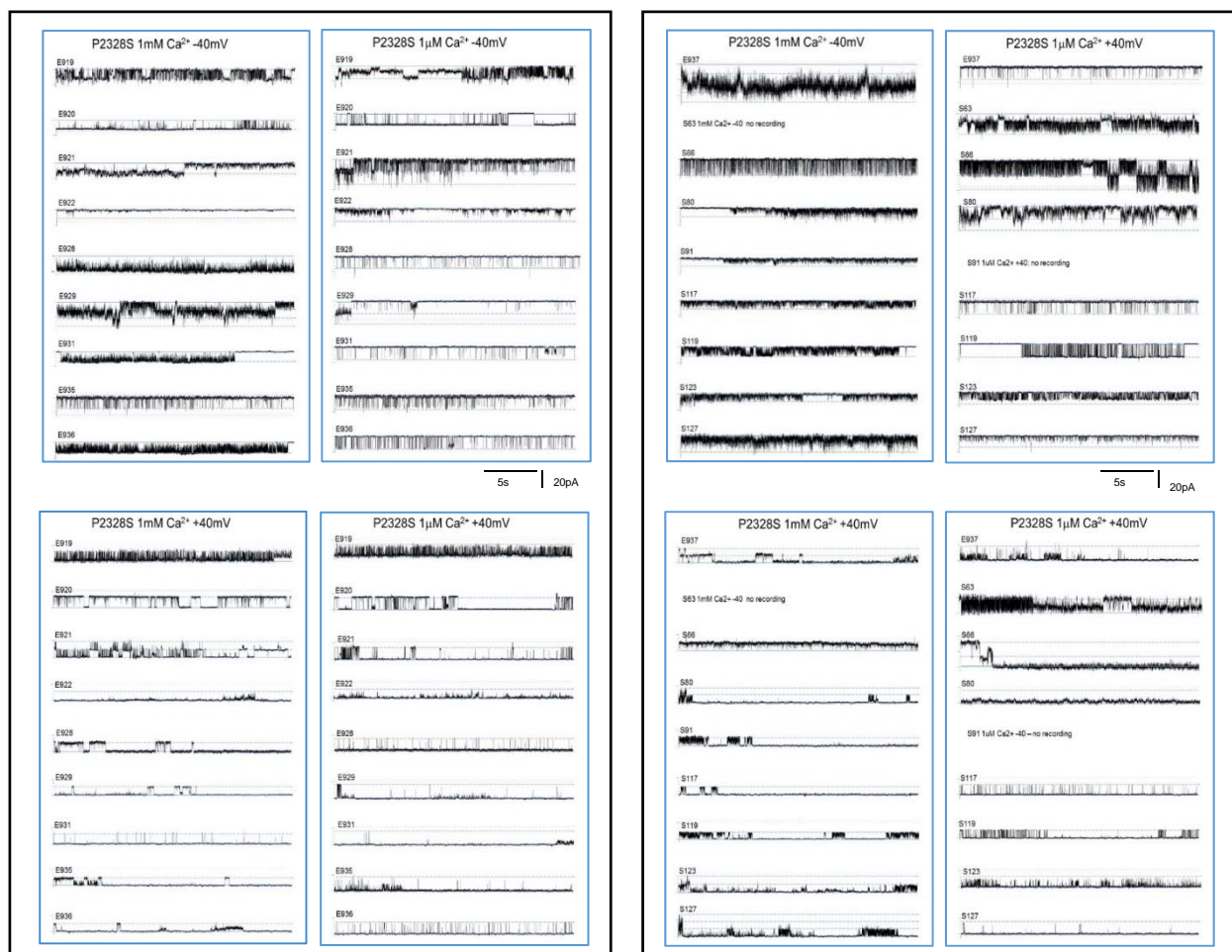


Figure S4. Examples of current recordings from 18 P2328S RyR2 channels used for analyses of channel activity with 1 mM and 1 μ M cytoplasmic Ca^{2+} presented in manuscript Figures 1 to 6. In each panel, records from the same channel are aligned horizontally to allow direct comparisons of the channel activity under each condition. Currents shown on the left hand side of each panel were recorded with 1 mM cytoplasmic Ca^{2+} , while those on the right hand side were recorded with 1 μ M cytoplasmic Ca^{2+} . Currents shown on the top half of each panel were recorded at -40 mV, while those in the lower half were recorded at +40 mV.